

Structural effects of C3 oxygenated fuels on soot formation in ethylene coflow diffusion flames

Yong Ren Tan^{1,2}, Maurin Salamanca^{1,2}, Jiaru Bai¹,
Jethro Akroyd^{1,2}, Markus Kraft^{1,2,3}

released: November 5, 2020

¹ Department of Chemical Engineering
and Biotechnology
University of Cambridge
Philippa Fawcett Drive
Cambridge, CB3 0AS
United Kingdom

² CARES
Cambridge Centre for Advanced
Research and Education in Singapore
1 Create Way
CREATE Tower, #05-05
Singapore, 138602

³ School of Chemical
and Biomedical Engineering
Nanyang Technological University
62 Nanyang Drive
Singapore, 637459

Preprint No. 261



Keywords: isopropanol (IPA), dimethoxymethane (DMM, OME1), dimethyl carbonate (DMC), soot formation, particle size distribution, synergistic effect

Edited by

Computational Modelling Group
Department of Chemical Engineering and Biotechnology
University of Cambridge
Philippa Fawcett Drive
Cambridge, CB3 0AS
United Kingdom

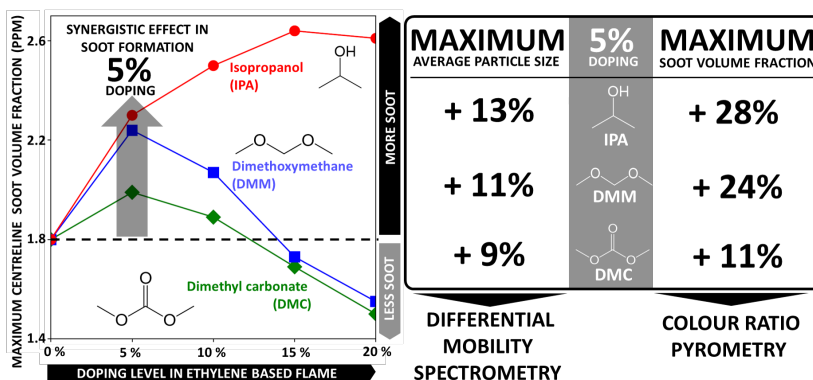
E-Mail: mk306@cam.ac.uk

World Wide Web: <https://como.ceb.cam.ac.uk/>



Abstract

This paper investigates how the structure of three C3 oxygenated fuels: dimethyl carbonate (DMC), dimethoxymethane (DMM) and isopropanol (IPA) influences soot formation when the fuels are blended with ethylene in laminar coflow diffusion flames. Up to 20% of the total carbon was substituted with oxygenated fuel. Colour ratio pyrometry was used to measure the soot volume fraction (SVF). IPA caused a strong increase in SVF, whereas DMM and DMC both caused an initial increase followed by a progressive decrease in SVF as the proportion of oxygenated fuel was increased. Differential mobility spectrometry and thermocouple probes were used to measure the particle size distribution and gas temperature in the flames at 5% blend strength. The hottest region of the 5% flames was consistently about 100 K cooler than the corresponding region of the ethylene flame, indicating a thermal effect of the doping. The 5% flames showed an increase in the maximum centre-line average particle size and SVF versus the ethylene flame, with the IPA showing the largest increase. The evolution of the centre-line particle size distributions showed that the 5% flames experienced earlier particle growth compared to the ethylene flame. Consideration of the role of the chemical pathways towards benzene formation suggests that methyl radicals from the decomposition of the oxygenated fuels are responsible for the increase in SVF at 5% doping. The difference in SVF between the IPA versus DMM and DMC flames is thought to be due to the additional presence of C3 species originating from the carbon-carbon bonded backbone of IPA. The difference between the DMC versus DMM flames is thought to arise from CO₂ produced during the decomposition of DMC, and a corresponding thermal effect where the pyrolysis region of the 5% DMC flame was observed to be about 50 K cooler than the other flames.



Highlights

- Soot formation studied in laminar diffusion flames doped with C3 oxygenated fuels
- Ethylene flame doped with up to 20% IPA, DMM or DMC at constant total carbon flow
- 5% doping increased soot volume fraction in the order IPA > DMM > DMC
- DMM and DMC decreased soot volume fraction at $\geq 15\%$ doping
- Effect explained in terms of molecular structure of oxygenated fuels

Contents

1	Introduction	3
2	Materials and methods	5
2.1	Laminar coflow diffusion flame	5
2.2	Soot volume fraction	6
2.3	Flame temperature	6
2.4	Soot particle size distribution	6
2.5	Kinetic modelling	7
3	Results and discussion	7
3.1	Visible flame length	8
3.2	Soot volume fraction	8
3.3	Flame temperature	9
3.4	Particle size distribution	11
3.5	Effect of C3 oxygenated fuels on soot formation	13
3.5.1	Effect of DMM and DMC on soot formation	14
3.5.2	Effect of IPA on soot formation	16
4	Conclusions	17
A	Supplementary materials	21
SM1.1	Visible flame lengths	21
SM1.2	Kinetic modelling	22
SM1.2.1	Ignition delay and laminar flame speed	22
SM1.2.2	Pyrolysis of fuel blends	23
SM1.2.3	Heating value and equilibrium temperature of fuel blends	24
	References	25

1 Introduction

The transport sector currently accounts for more than 60% of global oil consumption, corresponding to approximately 24% of global carbon dioxide emissions [1]. Passenger travel is expected to continue to rise in years to come, and hence the demand for energy from the transportation sector will follow suit [1]. Light-duty transportation can be quite straightforward to decarbonise by electrification. Nevertheless, aviation, long-distance transportation and shipping remain a challenge to achieve decarbonisation [2]. Carbon-neutral, sustainable, and energy-dense alternative liquid fuels may still play a critical role in keeping carbon dioxide emissions from these sectors in check [2, 3].

One of the most common and cost-effective sources of alternative liquid fuels is from the conversion of renewable resources [4, 5]. The use of non-fossil carbon in the production of these fuels means that they have a much lower carbon footprint than traditional fossil fuels [6], such that they are often referred to as carbon-neutral fuels, although it would be more accurate to refer to them as low-carbon fuels. In 2018, the total energy provided by such fuels was 3.7 exajoules (EJ), compared to the approximately 100 EJ consumed by the transport sector worldwide [7]. Ethanol from grain and sugar cane and biodiesel from oilseeds and waste oils remained the two categories of carbon-neutral fuels used at large scale currently [2, 7]. Some emerging carbon-neutral fuels such as dimethyl carbonate (DMC) [8, 9], dimethoxymethane (DMM) [10], isopropanol (IPA) [11] and poly(oxymethylene) dimethyl ether (PODE₃) [12] can be sourced sustainably. They have also shown promising performance when used in engines [13–15].

Blending carbon-neutral fuels with fossil-based fuels is a quick and simple strategy to start utilising alternative fuels that are sustainably-sourced [16, 17]. This strategy has also been adopted by governments where, for example, the European Parliament has proposed the Renewable Energy Directive II in December 2018 to increase the overall blending requirement on fuel distributors to a minimum of 14% for road and rail transport by 2030 [18, 19]. Vehicle manufacturers have also kept up with this trend by introducing flexible-fuel vehicles, which can operate with a variety of gasoline and ethanol fuel blends [20, 21].

Even though alternative fuels can be sustainably-sourced, the combustion of most fuels has the side effect of releasing particulate matter (commonly known as soot) into the atmosphere and causes harm to our health [22, 23] and environment [24–27]. Therefore, it is essential to understand how alternative fuels effect the generation of such particulate matter. In general, carbon-neutral fuels correspond to oxygenated fuels with different functional groups in their molecular structure, which are distinctively different from fossil-based fuels, and which influence their capacity to reduce soot emissions [21, 28–31]. Engine research reported in the literature has found that DMC [8, 13, 15, 32–34], IPA [14, 35–38] and DMM [15, 39–41] are promising oxygenated fuels that could reduce soot emissions. However, the emissions from engines are often governed by a combination of effects relating to the engine operating conditions and the chemical behaviour of the fuel. The influence of the fuel can be decoupled from the engine operating conditions by studying the fuel and the formation of soot precursors in a well-controlled fundamental combustion system such as a laminar coflow diffusion flame [42–45].

Fuels (gasoline, kerosene and diesel) and surrogate fuels [46, 47] contain a complex mix-

ture of hydrocarbons [48]. It is known that these fuel components decompose into small species such as CH_4 , C_2H_4 and C_3H_6 due to the low energy barrier of carbon-carbon β -scission of alkyl radicals when combusted [49–52]. For example, H_2 , CH_4 , C_2H_4 , and C_3H_6 were found to form in abundance during the pyrolysis of dodecane (one of the components of surrogate fuels [47]), with ethylene (C_2H_4) being the dominant species [53]. These small species, especially ethylene, play a key role in combustion [51, 52].

A synergistic effect on soot formation is sometimes observed during the combustion of fuel blends (*i.e.* fuels composed of a mixture of other fuels). This is defined as occurring when there is an increase in soot formation during the combustion of the fuel blend compared to the combustion of the individual fuels in the blend. This effect has been observed in fuel blends of containing oxygenated fuels [54–57]. The effect is understood to be influenced by the introduction of methyl ($\cdot\text{CH}_3$) radicals from the fuel blend into a base-fuel environment that is rich in C2 species (ethylene). This consequently leads to an enhancement of propargyl radical ($\cdot\text{C}_3\text{H}_3$) formation and eventually benzene production via $\cdot\text{C}_3\text{H}_3$ self-combination [44, 58]. The effect of the base-fuel environment was explored, where the addition of dimethyl ether to ethane and propane counterflow diffusion flames resulted in a monotonic decrease in sooting tendency, and where the synergistic effect was only observed with an ethylene base flame [54]. This synergistic effect is reported in several other investigations with dimethyl ether [55–57] and is attributed to the significant amount of methyl radicals formed when it decomposes during combustion.

Recently, the synergistic effect on soot formation was investigated in a laminar coflow diffusion flame when 5% PODE₃ ($\text{CH}_3 - [\text{OCH}_2]_3 - \text{OCH}_3$) was blended with ethylene [59]. Similar to the case with dimethyl ether, PODE₃ does not contain any carbon-carbon bonds and the synergistic effect was attributed to the introduction of methyl radicals from the decomposition of the PODE₃ into a rich C2 ethylene flame system. The impact of the molecular structure of the fuel on the synergistic effect in soot formation is therefore pivotal in the understanding of the changes induced by fuel blending. Moreover, it is important to take into account that in the combustion of alternative fuels, the oxygen-containing functional groups also play an essential role in determining the sooting tendencies [60]. There is a lack in the understanding of the effect of oxygen-containing functional groups on the synergistic effect in soot formation. In particular, insights on the soot formation of the oxygen-containing functional groups present in some of the emerging carbon-neutral fuels (DMC, DMM and IPA) is valuable when these fuels are considered as practical fuels in the near future.

The **purpose of this paper** is to understand the structural effects of different oxygenated fuels on soot formation. Three C3 oxygenated fuels were chosen in this investigation to represent three different oxygen-containing functional groups: carbonate ester (DMC), ether (DMM) and hydroxyl (IPA). The combustion of different strength blends of the oxygenated fuels with ethylene are investigated in a laminar coflow diffusion flame. Their effect on the soot formation process is investigated via soot volume fraction, thermocouple and particle size distribution (PSD) measurements. The impact of the different oxygen-containing functional groups and molecular structure in soot formation is critically assessed.

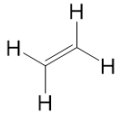
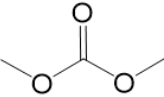
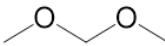
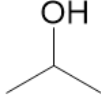
2 Materials and methods

This section provides a concise overview of the experimental setup and methods which were fully described in previous work [59].

2.1 Laminar coflow diffusion flame

Atmospheric-pressure laminar coflow diffusion flames were generated using a Yale steady Flame Burner [61]. The burner was chosen because it is one of the accepted target flame platforms adopted by the International Sooting Flame Workshop (ISF) for the study of soot formation [62]. In this study, thirteen flames were investigated. The first flame was a nitrogen diluted ethylene flame (60% C₂H₄:40% N₂). The other twelve flames were oxygenated fuel-blended ethylene flames. The following naming convention has been adopted for this investigation: The oxygenated fuels are specified as ‘DMC’ (dimethyl carbonate), ‘DMM’ (dimethoxymethane) and ‘IPA’ (isopropanol); followed by the percentage of total carbon contributed to the fuel mixture. **Table 1** shows the fuel flow rates for the flames studied in this work for each fuel blends.

Table 1: Fuel molecular structures and flow rates for the flames investigated.

Fuel blend	C ₂ H ₄ fuel flow rate (L _n /min)	DMC flow rate (g/h)	DMM flow rate (g/h)	IPA flow rate (g/h)
				
0%	0.147	0.00	0.00	0.00
5%	0.140	1.19	1.00	0.79
10%	0.133	2.37	2.00	1.58
15%	0.125	3.56	3.00	2.37
20%	0.118	4.74	4.01	3.16

The C₂H₄ flame corresponds to the ISF-targeted ISF-4 coflow 3 (Condition C) laminar diffusion flame [62]. The oxygenated fuels were blended with the C₂H₄ in different proportions while maintaining a constant carbon flow rate (9.49 g_c/h) and a constant cold gas coflow velocity (35 cm/s) for all flames. The ethylene and nitrogen were supplied from 99.99+% purity cylinders, and the air from an in-house compressor. DMC, DMM and IPA were procured from Tokyo Chemical Industry UK Ltd with a purity of at least 95% and used without further purification. The liquid fuel was evaporated and mixed with the ethylene and carrier gas in a Bronkhorst[®] Controlled Evaporator and Mixer (CEM). The fuel/carrier gas mixture was then fed to the burner via heated lines at 373 K. The flames were given 30 minutes to reach stability before performing any measurements. The measurement procedures are summarised below and are described in detail in previous work [59].

2.2 Soot volume fraction

The soot volume fraction, f_v , was measured using colour-ratio pyrometry [63, 64]. The measurement system has been described in detail previously [64]. In brief, a Blackfly S colour camera (BSF-U3-32S4C-C, FLIP Integrated Imaging Solutions Inc.) was paired with a Thorlabs MVL25M23 Lens to image the flames. A BG-7 filter from Thorlabs was used to balance the intensity ratios of the blue, green and red colour channels for the flame imaging [63]. For each flame, the captured images were then demosaiced and reconstructed, followed by the calculation of soot temperature and soot volume fraction using an in-house developed Python code [64]. The fitting the line-of-sight projection of a predefined intensity distribution (FLiPPID) method was employed to perform the reconstruction of the images (Abel inversion) [64]. Upon obtaining the soot temperature, the soot volume fraction for each flame was calculated as detailed in the literature [63].

2.3 Flame temperature

The flame temperature was measured using a rapid insertion method with an uncoated 125 μm Type-R thermocouple (Pt/Pt-13%R) [59, 65]. The details of the setup and measurement procedure were described previously [59, 66]. The gas temperature was obtained by applying a suitable radiation correction to the thermocouple data [67]. The uncertainty of the measurement is estimated to be $\pm 100\text{K}$.

2.4 Soot particle size distribution

The particle size distribution (PSD) of the electrical mobility diameter of the soot in the flame was measured using a DMS500 Differential Mobility Spectrometer from Cambusation Ltd. The detailed experimental setup for the PSD measurement can be found in our previous work [59]. The flame was sampled using a quartz probe with a tip length of 3 mm to minimise the residence time of the sample before dilution to quench post-sampling chemical reactions and to limit particle aggregation. The probe was supplied with a nitrogen dilution flow of 7.8 L_n/min from the DMS500 mass flow controller. Similar design of the probe has been used to extract samples from laminar coflow diffusion flames in other investigations [68, 69].

The sample volume drawn into the probe is controlled by adjusting a needle valve located between the probe and the DMS500. The dilution ratio as a function of the pressure drop for the sampling system was calibrated using an electrochemical oxygen sensor. The procedure to determine the dilution ratio is similar to those reported in the literature [70, 71] and was described in detail in our previous work [59]. In the current study, a room-probe pressure difference of $\Delta P = 28.0\text{--}33.0$ mbar was used to sample the flame. The pressure drop was chosen to minimise the flame perturbation while maintaining a first dilution ratio of at least 1200 and was sufficient to give reliable signal strength in the DMS500. The total dilution ratio (including the secondary dilution in the DMS500) in the current study was therefore at least 600,000, which is comfortably within the range suggested in the literature [70–72]. The PSD was measured and recorded for about 10 s

at each height above the burner (HAB) at a rate of 10 Hz, averaged and corrected by the dilution ratio. Each flame measurement was repeated four times and error bars showing the standard error are reported to exemplify the reproducibility of the experiments.

2.5 Kinetic modelling

Three kinetic models were established by combining different sub-mechanisms from the literature. The kinetic models were used to support the interpretation of the experimental results. It should be noted that the current work does not attempt to propose a new comprehensive model for each oxygenated fuel. Rather, it is the intention of the current study to use three kinetic models sharing the same core mechanism to analyse the combustion of the mixtures of the oxygenated fuels with ethylene.

The core mechanism is the USC-Mech II [73], consisting of 112 species and 785 reactions, including C0–C5 species. The USC-Mech II was chosen because it has been extensively calibrated to experimental measurements. The sub-mechanisms for DMM, DMC and IPA [74–76] were combined with the USC-Mech II model, ensuring that all three kinetic models use the same core mechanism. The total number of species and elementary reactions in the combined mechanisms were 137 chemical species and 874 elementary reactions in the USC-Mech II + DMC mechanism, 171 chemical species and 1036 elementary reactions in the USC-Mech II + DMM mechanism, and 123 chemical species and 855 elementary reactions in the USC-Mech II + IPA mechanism. The rate constants, thermodynamic and transport properties from the original mechanisms were used without any alterations. The kinetic models are available in CHEMKIN format in the Supplementary Material, accompanied by thermodynamic and transport properties.

The combined kinetic models were tested against experimental and modeling results of ignition delay [77] and laminar flame speed [78–80]. It was confirmed that the inclusion of the DMM, DMC and IPA sub-mechanisms does not compromise the ability of the mechanisms to describe the ethylene chemistry. The pyrolysis of each fuel mixture was simulated using the corresponding kinetic model with an imposed temperature profile from the corresponding flame experiment. Details of the simulation method and results can be found in Section SM1.2 of the Supplementary Material. The simulation results were used to help understand the effect of DMM, DMC and IPA on the chemistry leading to the formation of benzene.

3 Results and discussion

In this section, the experimental results from the thermocouple measurements, colour ratio pyrometry and differential mobility spectrometry of the oxygenated fuel-blended ethylene flames are presented and discussed. The synergistic effect of the selected oxygenated fuels on soot formation that is observed in the experimental results is explained in terms of the decomposition mechanisms of the different oxygenated fuels under fuel-rich conditions, supplemented with kinetic modelling results.

3.1 Visible flame length

The flames generated in the current study were all slightly lifted by 1.0 mm from the fuel tube, so minimising the heat loss from the flame to the fuel tube [81]. The flame lengths are reported in **Table 2**, and the corresponding flame images are shown in **Figure SM1.1**. The flame lengths were averaged over five frames.

Table 2: Visible flame lengths (mm) for the flames investigated with the associated standard error.

Fuel blends	DMC	DMM	IPA
0%	48.8 ±0.1	48.8 ±0.1	48.8 ±0.1
5%	49.4 ±0.2	50.3 ±0.1	52.1 ±0.2
10%	49.2 ±0.1	48.6 ±0.2	53.8 ±0.2
15%	46.7 ±0.1	48.1 ±0.6	53.0 ±0.1
20%	45.2 ±0.2	46.2 ±0.2	52.7 ±0.2

The C₂H₄ flame was observed to have a length of 48.4 mm, which agrees well with the reported flame length for the ISF standard flame [62]. The flame length increased compared to the C₂H₄ flame for all the cases with 5% oxygenated fuel. The IPA5 flame showed the largest increase and was observed to have a length of 52.1 mm, whilst the DMC5 flame showed the smallest increase and was observed to have a length of 49.4 mm. Two distinct behaviours were observed as the doping level was increased to 10%, 15% and 20%. DMC and DMM showed a progressive decrease in the flame length, whereas IPA flame increased in length to 53.8 mm at 10% blend strength, and then decreased slightly reaching a flame length of about 52.7 mm at 20% blend strength. The different flame lengths can be correlated to the soot volume fraction for each flame, see Section 3.2 for details.

3.2 Soot volume fraction

Figure 1 shows the soot volume fraction distributions measured using colour-ratio pyrometry. The maximum centre-line soot volume fraction of the C₂H₄ flame was measured as 1.8 ppm. In the literature, the value is reported as 1.2 ppm, which was measured using laser-induced incandescence [82]. Given that the uncertainty bounds along the centre-line of the flame are ±10% when using the FLiPPID method to process colour-ratio pyrometry data [64] and that the difference between colour-ratio pyrometry and laser-induced incandescence measurements is typically ±15% [63, 83, 84], the current measurement is considered to be reasonable. At the wings of the C₂H₄ flame, the maximum soot volume fraction was measured as 2.0 ppm at the wings, consistent with the value of 1.8 ppm measured using laser-induced incandescence [83].

The maximum centre-line soot volume fractions are shown in **Figure 2**. In all cases, the presence of 5% oxygenated fuel causes an increase in the maximum centre-line soot volume fraction compared to the C₂H₄ flame. The IPA5 and DMM5 flames show almost

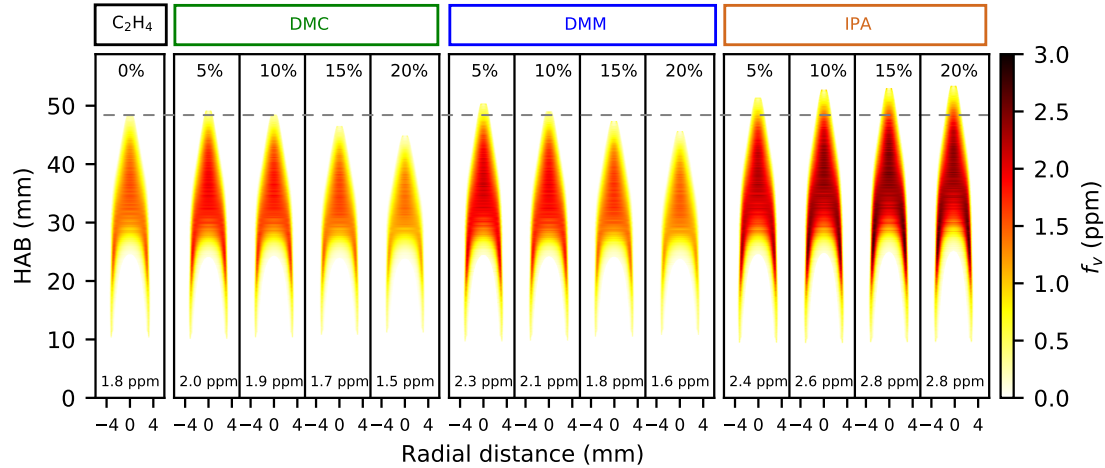


Figure 1: Soot volume fraction, f_v , distributions measured using colour-ratio pyrometry. The centre-line maximum soot volume fraction for each flame is indicated at the bottom each flame. The percentage of DMC, DMM and IPA in each fuel blend is indicated at the top of each image. The grey dotted horizontal line indicates the length of C_2H_4 flame.

double the increase observed in the DMC5 flame (28% and 24% versus 11% respectively). As the proportion of oxygenated fuel in the blend is increased, the maximum soot volume fraction continues to increase in the IPA flames, reaching approximately 2.6 ppm in the IPA20 flame, corresponding to a 47% increase compared to the C_2H_4 flame. In contrast, the DMM and DMC flames show a progressive decrease in the maximum centre-line soot volume fraction. The larger maximum soot volume fraction observed in the DMM compared to the DMC flame persists in the 10% blend, but is no longer apparent by the time the blend reaches 15% and 20%. These observations are in good agreement with the trends observed in the flame length.

As shown in Figure 1 and 2, the blending of 5% oxygenated fuel with the ethylene increases the centre-line maximum soot volume fraction. This suggests a synergistic effect in the soot formation, which is further investigated in terms of the flame temperature and particle size distribution.

3.3 Flame temperature

Figure 3 shows the measured centre-line flame temperature, average particle size and centre-line soot volume fraction of the C_2H_4 flame and 5% blended flames. The data are presented in terms of a non-dimensional axial position (NDAP) to enable comparison of the effect of the oxygenated fuels across all the flames with varying flame lengths. NDAP has been used in the literature to establish chemical species and temperature correlations between flames of different lengths [85, 86]. The figure is divided into four regions, labelled A–D and demarcated by vertical dashed lines, to facilitate discussion.

The experimental temperature profile and maximum temperature measured in the current

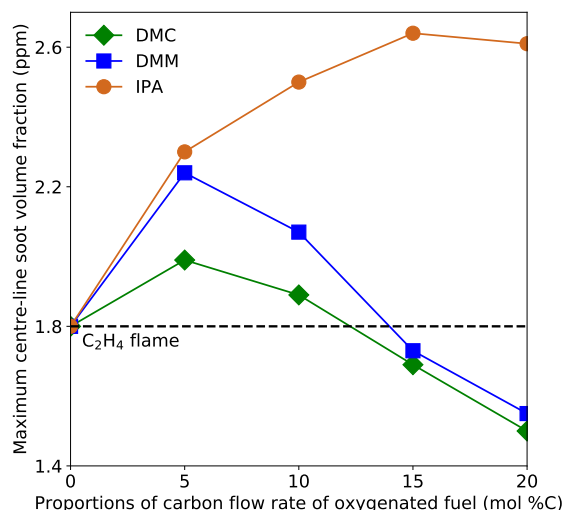


Figure 2: Maximum centre-line soot volume fractions as a function of the percentage of the total carbon flow rate of oxygenated fuel added to the flame.

study were consistent with measurements reported in the literature for the C_2H_4 flame [87, 88]. The centre-line flame temperature profiles are quite similar across all the flames and increase with NDAP in Region A (NDAP = 0.1–0.5). The temperature of the DMC5 flame is approximately 50 K lower than for the other flames. This is likely due to the presence of carbon dioxide from the DMC decomposition in the pyrolysis region (this will be discussed further in Section 3.5) [89]. This difference in temperature means that a combination of temperature and chemical effects will affect the soot formation in the DMC5 flame [89, 90]. The similarity of the centre-line temperatures in the C_2H_4 , DMM5 and IPA5 suggests that the chemistry will play a more significant role in determining the differences in the sooting behaviour of these flames.

The measured centre-line flame temperatures of all the flames show a slight dip followed by a region of approximately constant temperature in Region B (NDAP = 0.50–0.78). This is not uncommon and has been observed in the literature [85, 86, 91–96], and is attributed to the radiative heat loss from the flame due to the soot [97]. At the boundary with Region C (NDAP = 0.78–1.0), the measured temperature of all of the flames increases rapidly, with the temperature increasing to a maximum that defines the boundary with Region D at NDAP = 1.0.

In Region C, the measured temperature profiles of the 5% blended flames are very similar and are consistently about 100 K lower than that of C_2H_4 flame. The difference from the C_2H_4 flame is not reflected in the heating values of the fuels nor in the equilibrium temperature of stoichiometric mixtures of the fuels and air (see Section SM1.2.3 of the Supplementary Material). The similarity in the temperature profiles of blended flames is also not reflected in the soot volume fraction profiles, which are quite distinct, both from the C_2H_4 flame and from each other.

3.4 Particle size distribution

The average particle size along the centre-line (top panel of Figure 3) increases slowly in Region A, with the 5% blended flames showing slightly larger average particle size than the C_2H_4 flame. No signal is observed for the soot volume fraction (bottom panel of Figure 3) as it is below the lower limit of detection of the pyrometry technique. A rapid increase in the average particle size and soot volume fraction is observed in Region B in all flames. The average particle size and centre-line soot volume fraction of the 5%

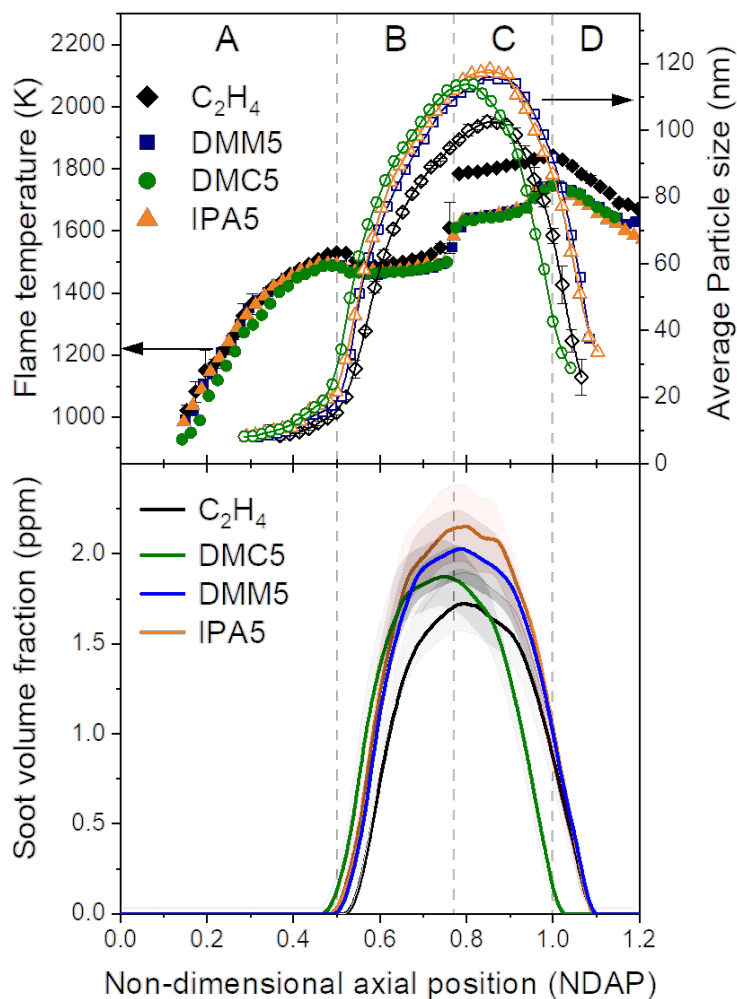


Figure 3: *Top left axis: Radiation-corrected temperatures measured using a thermocouple along the centre-line of the C_2H_4 , DMC5, DMM5 and IPA5 flames. Top right axis: Average particle size distribution measured along the centre-line of the C_2H_4 , DMC5, DMM5 and IPA5 flames using the DMS500. The error bars show the standard error for the C_2H_4 flame and are calculated over at least three repeats of the measurements. Error bars are not shown for the DMC5, DMM5 and IPA5 flames, but are similar in size to those for the C_2H_4 flame. Bottom left axis: Centre-line soot volume fraction of the C_2H_4 , DMC5, DMM5 and IPA5 flames.*

blended flames remain larger than those in the C_2H_4 flame.

The maximum centre-line average particle size and soot volume fraction are observed in the early part of in Region C, after which they decrease rapidly throughout the remainder of Region C and D. The 5% blended flames have a larger maximum average particle size than the C_2H_4 flame, with the maximum average particle sizes and percentage differences following in the order 118 nm (IPA5, 13% larger), 116 nm (DMM5, 11% larger), 114 nm (DMC5, 9% larger) versus 103 nm in the C_2H_4 flame. This is consistent with the trends in the visible flame length (Table 2) and the maximum centre-line soot volume fraction (Figure 2). However, the *locations* where the maxima are observed do not follow such a direct trend. The IPA5 and DMM5 flames both show the maximum centre-line average particle size at NDAP = 0.85 (the middle of Region C), similar to the C_2H_4 flame, whereas the DMC5 flame shows the maximum at NDAP = 0.82, slightly earlier than the other flames. Likewise, the C_2H_4 , IPA5, and DMM5 flames show the maximum centre-line soot volume fraction at NDAP = 0.8, whereas the DMC5 flame shows the maximum slightly earlier at NDAP = 0.76. The reasons for this are explored in Section 3.5.1.

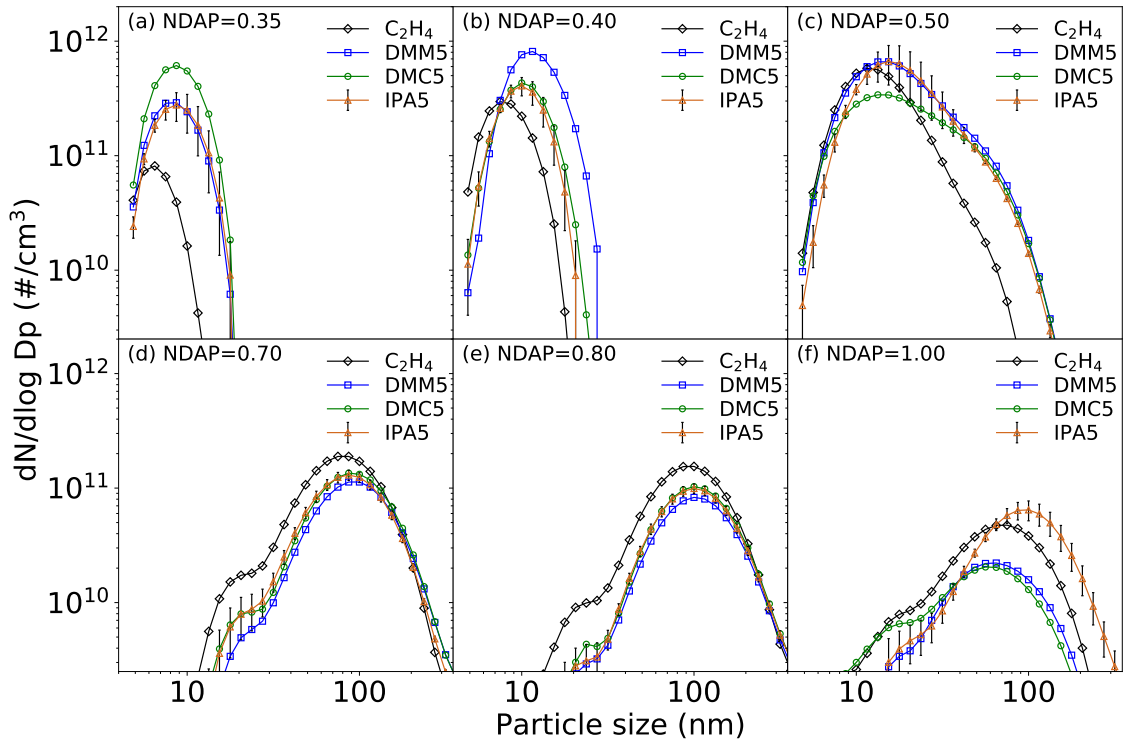


Figure 4: Particle size distributions measured using the DMS500 along the centre-line of the C_2H_4 , DMC5, DMM5 and IPA5 flames. The data in each panel are grouped by non-dimensional axial position (NDAP). The error bars show the standard error of the measurements at each position over four repeats.

Figure 4 shows the full particle size distributions (PSDs) of the C_2H_4 , DMC5, DMM5 and IPA5 flames at different non-dimensional axial positions (NDAP). The evolution of the peak number density of the PSDs provides a deeper insight into the changes in the soot formation process due to the addition of the oxygenated fuels to the 5% blended flames.

Figures 4(a) and (b) show that all the flames have unimodal distributions characteristic of nucleation with particles sizes less than 30 nm for $NDAP \leq 0.40$. The 5% blended flames show larger peak number densities and broader size distributions occurring earlier than for the C_2H_4 flame, indicating earlier nucleation and growth, with the maximum number density and therefore the nucleation occurring earliest in the DMC5 flame.

Figure 4(c) shows that the particles are starting to transition to bimodal size distributions by $NDAP = 0.5$. For example, the PSD for the C_2H_4 flame has a peak number density at a size of about 15 nm, whilst also showing a shoulder at about 70 nm. The shoulders are more pronounced in the 5% blended flames, consistent with the particles experiencing earlier growth and an earlier transition to bimodal PSDs than in the C_2H_4 flame.

Figures 4(d)–(f) show that the bimodal PSDs are well-established for $NDAP \geq 0.70$, with the PSDs showing a weak mode below 30 nm and a strong accumulation mode in the range 40–300 nm. In all cases, the peak number density is achieved before $NDAP = 0.70$ and continues to decrease with $NDAP$. The number densities of the 5% blended flames are consistently lower than that of the C_2H_4 flame (except for the largest particles in the IPA5 flame at $NDAP = 1.0$), indicating earlier oxidation of the particles. A similar trend was observed in analogous flames with a 5% blend of $PODE_3$ [59].

3.5 Effect of C3 oxygenated fuels on soot formation

Understanding the effect of the fuel on soot formation is important in fuel design and in developing strategies to reduce soot emissions [98, 99]. The formation of benzene is generally believed to be the rate-limiting step in the formation of the polycyclic aromatic hydrocarbons that ultimately leads to the formation of soot [100–104]. Several reactions involving small unsaturated hydrocarbon radicals are considered as possible pathways for the formation of benzene [104]. Within these pathways, resonance-stabilised radicals (RSRs) are known to be important in the production of the first aromatic ring [42, 104], in particular $\cdot C_3H_3$, $i\text{-}\cdot C_4H_3$, $i\text{-}\cdot C_4H_5$ and $\cdot C_5H_5$ [101, 105–110]. The level stabilisation is such that reactions between RSRs can proceed quickly [105], but that RSRs can exist at higher concentrations than non-resonantly stabilised radicals in flames [42, 104, 111]. The consideration of pathways for the formation of benzene via RSRs is therefore critical in understanding the how different fuels effect soot formation [104].

Figure 5 shows the major reaction pathways involving ethylene, DMM, DMC and IPA leading to the formation of benzene [74, 75, 101, 105, 112–115]. The species in the figure are numbered to facilitate the ensuing discussion. The pathways can be categorised into odd (C3+C3 and C5+C1) and even (C4+C2) pathways [104]. Hydrogen abstraction from ethylene (111 kcal/mol bond energy) is more energetically favourable than carbon-carbon double bond cleavage (174 kcal/mol) [116]. The hydrogen abstraction produces species including vinyl radicals ($\cdot C_2H_3$), acetylene (C_2H_2) and ethynyl radicals ($\cdot C_2H$) [112, 113] that can combine to form C4 species [112, 113, 117] including $i\text{-}\cdot C_4H_3$ and $i\text{-}\cdot C_4H_5$. These are both C4 RSRs that can be easily produced from their corresponding *n*-isomers through H-atom-assisted isomerisation in the fuel-rich regions of the current flames [105, 118]. In the presence of C2 species, these C4 RSRs can provide a major route for the formation of benzene via the C2+C4 pathway [106, 119]. In the ethylene flame, the concentration

of C2 and C4 species dominates compared to C1 species [118, 120]. This is reflected in the pyrolysis simulation results (see Section SM1.2.2 of the Supplementary Material), where Figures SM1.4(g) and (h) show that the C1 species mole fractions are lower and Figures SM1.4(k) and (l) show that the C4 species mole fractions are higher for pyrolysis of ethylene than for all the mixtures containing oxygenated fuels.

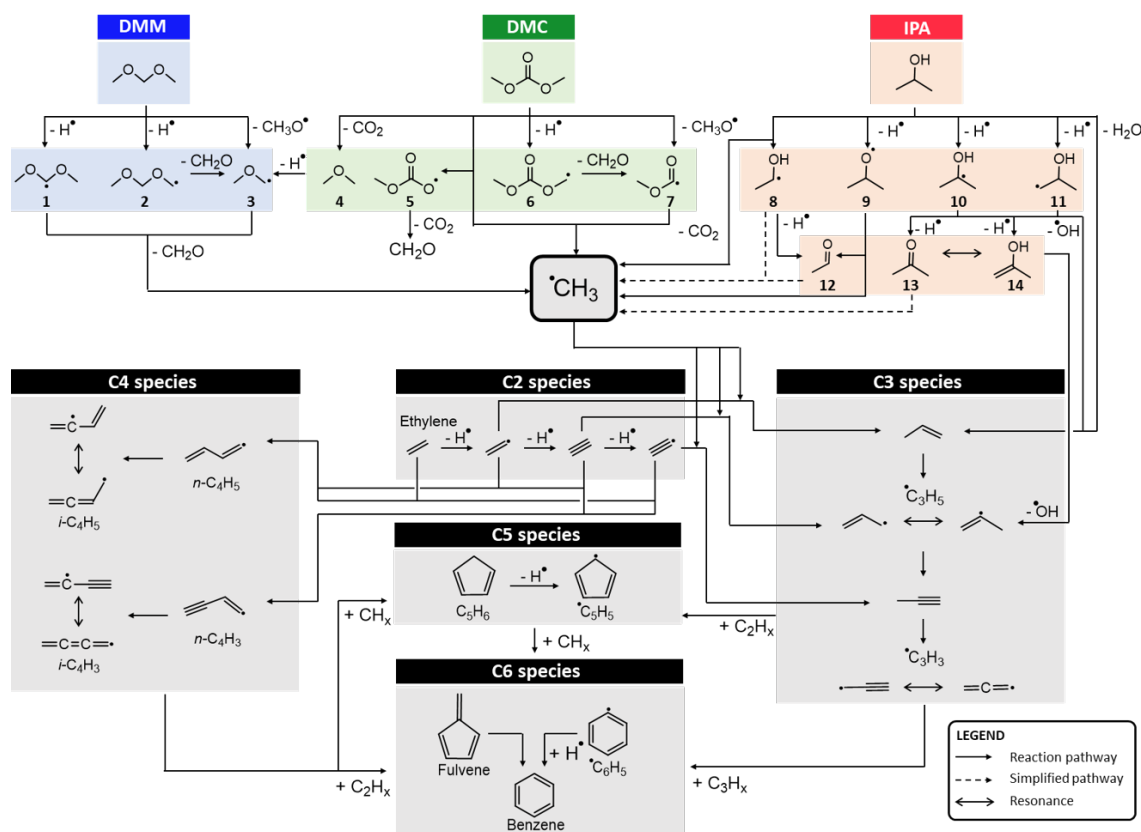


Figure 5: Mechanism pathways for benzene formation from dimethylcarbonate (DMC), dimethoxymethane (DMM), isopropanol (IPA) and ethylene. Ethylene combustion normally follow a C₄+C₂ pathway towards the formation of benzene. DMC, DMM and IPA decompose to form methyl radicals that can react with ethylene to activate C₃ and C₅ pathways towards benzene formation.

The following sections describe how doping ethylene flames with DMM, DMC and IPA effects the pathways leading to the formation of benzene. **Figure 6** shows the structure of DMM, DMC and IPA, along with annotations and bond dissociation energies to facilitate the discussion.

3.5.1 Effect of DMM and DMC on soot formation

DMM and DMC have several similarities in terms of their molecular structure and how they decompose, both providing a source of methyl radicals.

DMM can decompose through hydrogen abstraction and carbon-oxygen scission reactions [74]. Hydrogen abstraction can occur at the α and β carbon-hydrogen bonds, both

of which have similar bond dissociation energies, as shown in Figure 6 [121]. Consideration of the number of α and β carbon-hydrogen bonds suggests that hydrogen abstraction at the α bond may occur more frequently. The resultant dimethoxymethyl (**1**) and methoxymethoxymethyl (**2**) radicals can decompose to form methyl ($\cdot\text{CH}_3$) radicals and formaldehyde (CH_2O) [74]. Similarly, two consecutive carbon-oxygen bond scissions can produce methyl radicals and formaldehyde [74] via methoxymethyl (**3**).

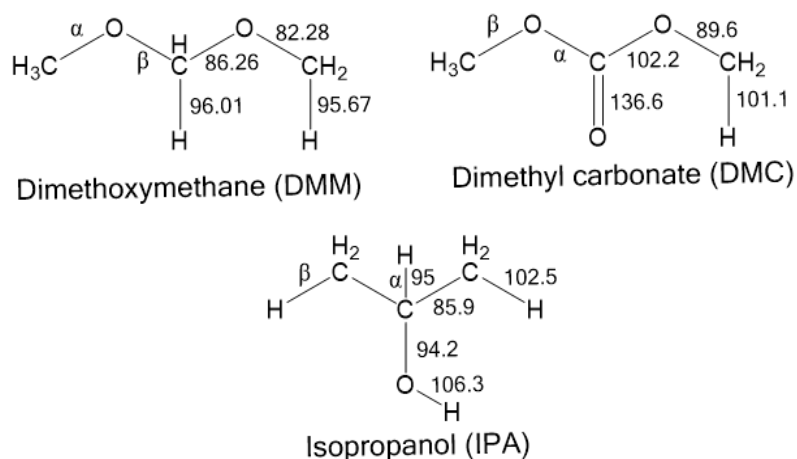


Figure 6: Structure of dimethoxymethane (DMM), dimethyl carbonate (DMC) and isopropanol (IPA). The numbers refer to bond dissociation energies for DMM [121], DMC [75, 122] and IPA [123] in units of kcal/mol.

DMC can decompose via three pathways: decarboxylation, carbon-oxygen bond dissociation and hydrogen abstraction [75], with significant formation of carbon dioxide [122]. The decarboxylation produces carbon dioxide and dimethyl ether (**4**), which subsequently undergoes hydrogen abstraction and carbon-oxygen bond scission to form methyl radicals and formaldehyde [75]. The carbon-oxygen bond dissociation can happen at either the α or the β carbon-oxygen bond from the carbonyl group, with the bond dissociation energies suggesting that the dissociation may favour the β more than the α carbon-oxygen bond. The hydrogen abstraction produces $\text{CH}_3\text{OCOOCH}_2\cdot$ (**6**) radicals which can decompose into methyl radicals and carbon dioxide.

The soot volume fraction and maximum average particle size (Figures 2 and 3) are observed to increase in the DMM5 and DMC5 flames compared to the C_2H_4 flame. The dopants provide a source of methyl radicals, which can react with ethynyl radicals ($\cdot\text{C}_2\text{H}$) to form methylacetylene (C_3H_4) and, after subsequent a hydrogen abstraction, propargyl ($\cdot\text{C}_3\text{H}_3$) radicals. Propargyl is a RSR and can self-recombine relatively quickly in a combustion environment [112] to form benzene via the C3+C3 pathway [42, 101, 105, 124]. The presence of C3 species also enables benzene formation via the C5+C1 pathway (involving the RSR $\cdot\text{C}_5\text{H}_5$) [105, 125, 126]. It is thought that it is the availability of methyl radicals and the consequent formation of benzene via the odd pathways, in addition to the even pathways that dominate in the C_2H_4 flame, that is responsible for the synergistic increase in soot production in the DMM5 and DMC5 flames. This is reflected in the pyrolysis simulation results (see Section SM1.2.2 of the Supplementary Material), where Figures SM1.4(g)–(j) and (m) show that the species that contribute to the odd pathways

have species mole fractions that are consistently higher than in the C₂H₄ flame.

The soot volume fraction and maximum average particle size (Figures 2 and 3) are observed to decrease as the level of DMM and DMC is increased from 5% to 10%, 15% and 20%. This is interpreted as indicating a decrease in the rate of formation of benzene, despite the increase in the concentration of methyl radicals likely to result from increased doping with DMM and DMC. It is apparent that the additional methyl radicals originating from the DMC and DMM are less important at higher blend strengths. What makes this situation distinct from the 5% flames is that the odd pathways are already open. Given that the total carbon mass flow remains constant, the additional DMM and DMC results in a decrease in the mass flow of C₂ species supplied via the ethylene part of the fuel mixture. This is unfavourable for benzene formation because not all of the carbon provided by the oxygenated fuel participates in soot production, but instead forms carbon monoxide (via formaldehyde, CH₂O) [122, 127] and carbon dioxide (in the case of DMC) as the oxygenated fuel decomposes. These observations are consistent with the literature, where C₂H₄ flames have been doped with dimethyl ether [55], POE₃ (CH₃ - OCH₂ - OCH₃) [59], methane [128] and ethanol [129]. The effect of methyl radicals from the dopants was found to be critical in understanding the non-monotonic change in benzene and soot formation.

A further observation is that the DMC flames are less sooting than the DMM flames. For example, the DMC flames show lower maximum centre-line soot volume fractions and the DMC5 flame shows a smaller maximum centre-line average particle size than the corresponding DMM flames. It is possible that this is due to the formation of carbon dioxide during the decomposition of DMC. This may reduce the synergistic effect in soot formation through thermal and chemical effects [90, 130, 131]. The thermal effect is evident from the lower flame temperature of the DMC5 flame in Region A of Figure 3. Meanwhile, the chemical effect may arise via the increased consumption of hydrogen radicals in CO₂ + H ⇌ CO + OH reactions [130, 131], leading to a reduction in the H-abstraction-C₂H₂-addition (HACA) growth of polycyclic aromatic hydrocarbons [100, 132, 133].

3.5.2 Effect of IPA on soot formation

IPA can decompose via dehydration, hydrogen abstraction + β-scission, carbon-oxygen bond dissociation and carbon-carbon bond dissociation [114, 134]. The main decomposition species are methyl radicals, water and C₃ species; markedly different from DMM and DMC. In particular, the dehydration of IPA leading to the formation of C₃H₆ and water may be more significant than other decomposition pathways [114]. This is reflected in the pyrolysis simulation results (see Section SM1.2.2 of the Supplementary Material), where Figures SM1.4(d) and (i) show that water and C₃H₆ are produced in higher amounts by the IPA fuel blend compared to the DMM and DMC blends. The water is not thought to have a significant chemical effect on the growth of soot [130]. There are three possible sites for hydrogen abstraction: the carbon-hydrogen bond α to the hydroxyl group, the carbon-hydrogen bond β to the hydroxyl group and the oxygen-hydrogen bond in the hydroxyl group, where consideration of the bond dissociation energies suggests that hydrogen abstraction at the carbon-hydrogen bond α to the hydroxyl group (95.0 kcal/mol)

is most favourable [114, 134]. The bond dissociation energies of the carbon-carbon (85.9 kcal/mol) and carbon-oxygen (94.2 kcal/mol) bonds [123] suggest that cleavage of both these bonds is more favorable than hydrogen abstraction.

The soot volume fraction and maximum average particle size (Figures 2 and 3) are observed to be larger in the IPA flames compared to all the other flames. In contrast to DMM and DMC, the C-C bonded backbone of IPA is such that the decomposition of IPA produces C3 in addition to C1 species, enabling the direct formation of benzene via the C3+C3 pathway [112]. The C3 species can also easily react with C2 species from ethylene to form C5 species, promoting the C5+C1 pathway [135, 136]. The C5+C1 pathway involving cyclopentadienyl ($\cdot\text{C}_5\text{H}_5$) RSRs and methyl radicals has been shown to have a significant role in the formation of benzene [108–110, 136]. The radicals can react to form fulvene, followed by ring-enlargement reactions to provide a fast route to benzene [109, 110, 115]. In addition, the recombination of $\cdot\text{C}_5\text{H}_5$ RSRs can directly form naphthalene [137, 138], which may also be an important reaction that increases the rate of formation of larger polycyclic aromatic hydrocarbons in IPA flames [137, 138].

The increase in the soot volume fraction observed up to 15% IPA blending in Figure 2 suggests a continued increase in the rate of benzene formation. It is postulated the reason for the difference in behaviour from the DMM and DMC flames is the direct access to C3 species that arises as a consequence of the C-C bonded backbone of IPA. When the proportion of IPA is increased, the increased abundance of C3 species (more than) compensates for the reduction in C2 species due to displacement of ethylene. This is in marked contrast to DMM and DMC, where the displacement of C2 species from the ethylene eventually leads to a decrease in soot formation. The slight decrease in soot volume fraction as the IPA blend strength is increased from 15% to 20% is potentially due to the action of hydroxyl ($\cdot\text{OH}$) radicals resulting from the dissociation of the carbon-oxygen bond in the IPA. The presence of low concentrations of $\cdot\text{OH}$ radicals will promote hydrogen abstraction reactions, leading to the formation of water and an increase in the H-abstraction- C_2H_2 -addition (HACA) growth of polycyclic aromatic hydrocarbons [100, 132, 133] and a consequent increase in soot production. However, if the blend strength is increased high enough, the presence of high concentrations of $\cdot\text{OH}$ radicals is expected to promote oxidation, leading to a net decrease in the rate of production of soot [42, 134].

4 Conclusions

In this work, the effect of the molecular structure of different C3 oxygenated fuels on soot formation was investigated in laminar coflow diffusion flames. Three C3 oxygenated fuels were chosen to represent different oxygen-containing functional groups: carbonate ester (dimethyl carbonate, DMC), ether (dimethoxymethane, DMM) and hydroxyl (isopropanol, IPA). The oxygenated fuels were blended with ethylene at 5%, 10%, 15% and 20% of the total carbon flow rate to enable oxygenated fuel-blended flames with constant carbon flow rate. Colour ratio pyrometry was used to study the effect of the fuel blend on the soot volume fraction. Differential mobility spectrometry and thermocouple measurements were used to investigate the particle size distribution of the soot and temperature of the flame as a function of the height above burner in the flames with the 5% blends.

At 5% blending, the maximum centre-line soot volume fraction and maximum centre-line average particle increased compared to the pure ethylene flame. The percentage increases were 13%, 11% and 9% in the maximum centre-line soot volume fraction, and 28%, 24% and 11% in the the maximum centre-line average particle size for the IPA, DMM and DMC blends respectively. The maximum centre-line soot volume fraction showed two distinct trends with increasing blend strength (up to 20%). IPA caused a strong increase in the maximum centre-line soot volume fraction up to 15% blend strength followed by a small decrease between 15% and 20% blend strength, while DMM and DMC both caused a progressive decrease in the maximum centre-line soot volume fraction as the blend strength increased from 5% to 10%, 15% and 20%.

The effect of the different fuel blends on the soot production in the flames can be explained in terms of the molecular structure of the oxygenated fuels. Consideration of the decomposition pathways suggests that the oxygenated fuels provide a source of methyl radicals. In the case of the 5% blends, it is believed that the introduction of methyl radicals (from the oxygenated fuels) into an environment that is rich in C2 species (from the ethylene) promotes soot growth by enabling the formation of benzene via C3+C3 and C5+C1 pathways in addition to C2+C4 pathways. In the case of DMM and DMC, it is believed that the reduction in soot at higher blend strengths is due to carbon from the oxygenated fuels displacing carbon from the ethylene. This results in a decrease in the carbon available for the C2+C4 pathways and an increase in the proportion of carbon that does not participate in soot production, but that forms carbon monoxide and carbon dioxide (in the case of DMC) during the decomposition of the oxygenated fuel. In the case of IPA, it is believed that the increase in soot production with blend strength is due to the presence of the C3 carbon-carbon bonded backbone, which results in a number of C3 decomposition products. This enables direct access to benzene formation via the C3+C3 pathways (as opposed to DMM and DMC, which access the C3 pathways via C1 species). This more than compensates for the decrease in the carbon available for the C2+C4 pathways, such that the IPA-doped flames produce more soot than any of the other flames.

The differences in the molecular structure of the fuels also induces thermal differences in the flames. Temperature measurements show that the pyrolysis region (NDAP = 0.1–0.5) of the 5% DMC flame is approximately 50 K cooler than the corresponding region of the 5% DMM, 5% IPA and ethylene flames, and that the hottest region of the 5% flames (NDAP = 0.78–1.0) is consistently about 100 K cooler than the ethylene flame.

Acknowledgements

This research was supported by the National Research Foundation, Prime Minister's Office, Singapore under its Campus for Research Excellence and Technological Enterprise (CREATE) programme. Y. R. Tan acknowledges financial support provided by Fitzwilliam College Cambridge, Trinity College Cambridge and the Cambridge Trust. J. Bai acknowledges financial support provided by CSC Cambridge International Scholarship from Cambridge Trust and China Scholarship Council. M. Kraft gratefully acknowledges the support of the Alexander von Humboldt Foundation.

The authors would like to thank Wenyu Sun from the Institut de Combustion Aérother-

mique Réactivité et Environnement (ICARE), CNRS Orleans Campus; Bing Yang from the Center for Combustion Energy and the Department of Energy and Power Engineering, Tsinghua University; Lorena Marrodán from Universidad Zaragoza for providing the data that assisted in the simulation; Chiara Saggese from Lawrence Livermore National Laboratory and Scott S. Goldsborough from Argonne National Laboratory for providing the isopropanol submechanism.

A Supplementary materials

SM1.1 Visible flame lengths

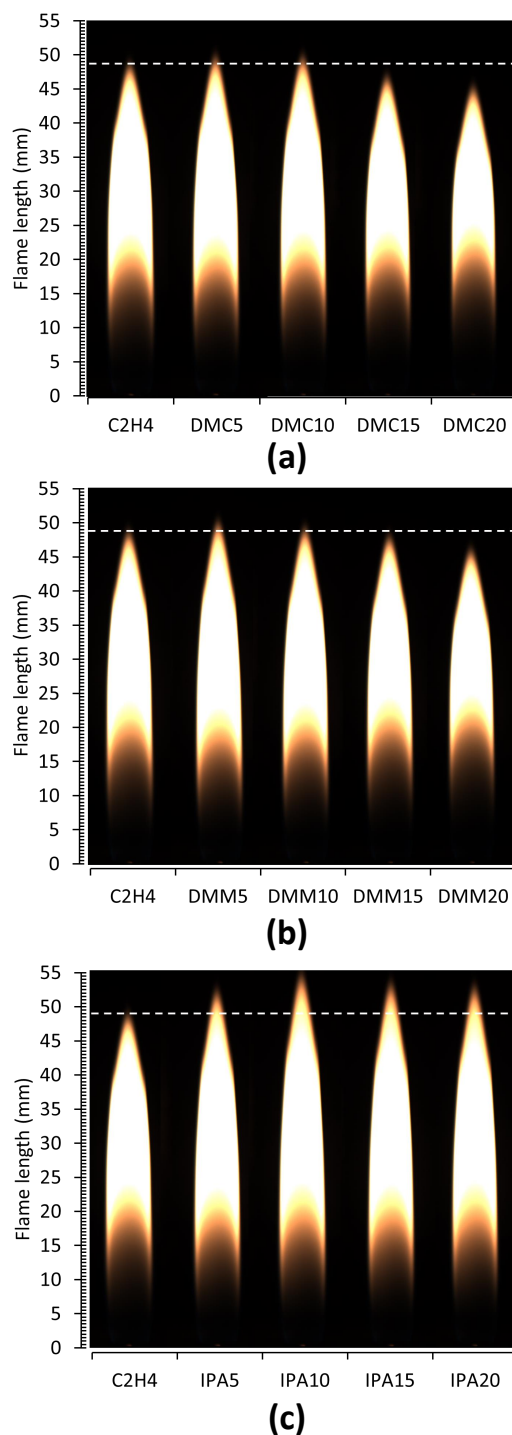


Figure SM1.1: Visible flame lengths. The images were taken with the same exposure time (0.002 s), aperture opening (full opening) and colour balance ratio (red:blue = 1.0:2.6). The white line indicates the length of C_2H_4 flame.

SM1.2 Kinetic modelling

SM1.2.1 Ignition delay and laminar flame speed

Three new kinetic models were created by combining the USC-MECH II mechanism [73] with three sub-mechanisms for dimethoxymethane (DMM) [74], dimethyl carbonate (DMC) [75] and isopropanol (IPA) [76], as described in Section 2.5 of the main text.

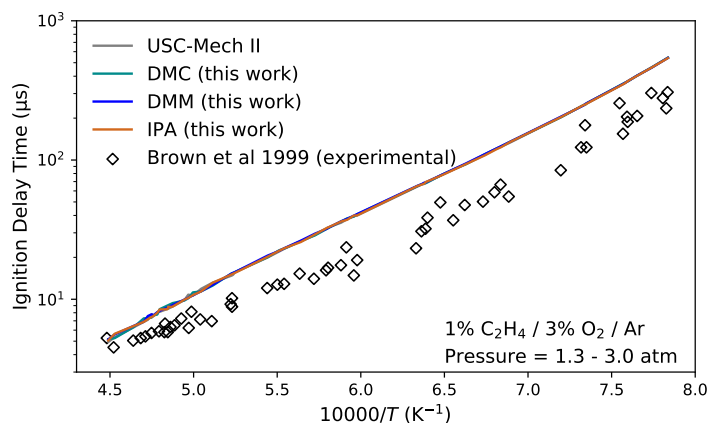


Figure SM1.2: Ignition delay versus reciprocal temperature.

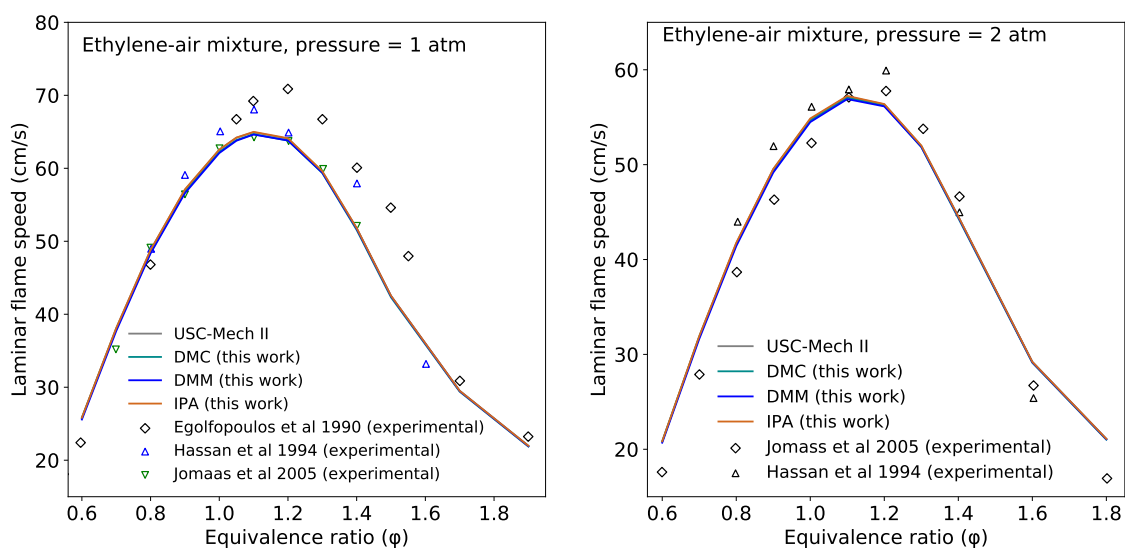


Figure SM1.3: Laminar flame speed versus equivalence ratio of ethylene in air.

The performance of the mechanisms was verified by checking that they could reproduce experimental data for the ignition delay [77] and laminar flame speed [78–80] of ethylene. The simulations were performed using the kinetics & SRM Engine Suite software (version 2020.1.1) [139] (ignition delay) and Cantera (version 2.4.0) [140] (laminar flame speed). Figures SM1.2 and SM1.3 show that the simulations remain in good agreement with the experimental data and confirm that the addition of the DMC, DMM and IPA chemistry does not compromise the ability of the mechanisms to describe ethylene combustion.

SM1.2.2 Pyrolysis of fuel blends

Figure SM1.4 shows the results of simulations of the pyrolysis of the fuel blends from the C_2H_4 , DMM5, DMC5 and IPA5 flames.

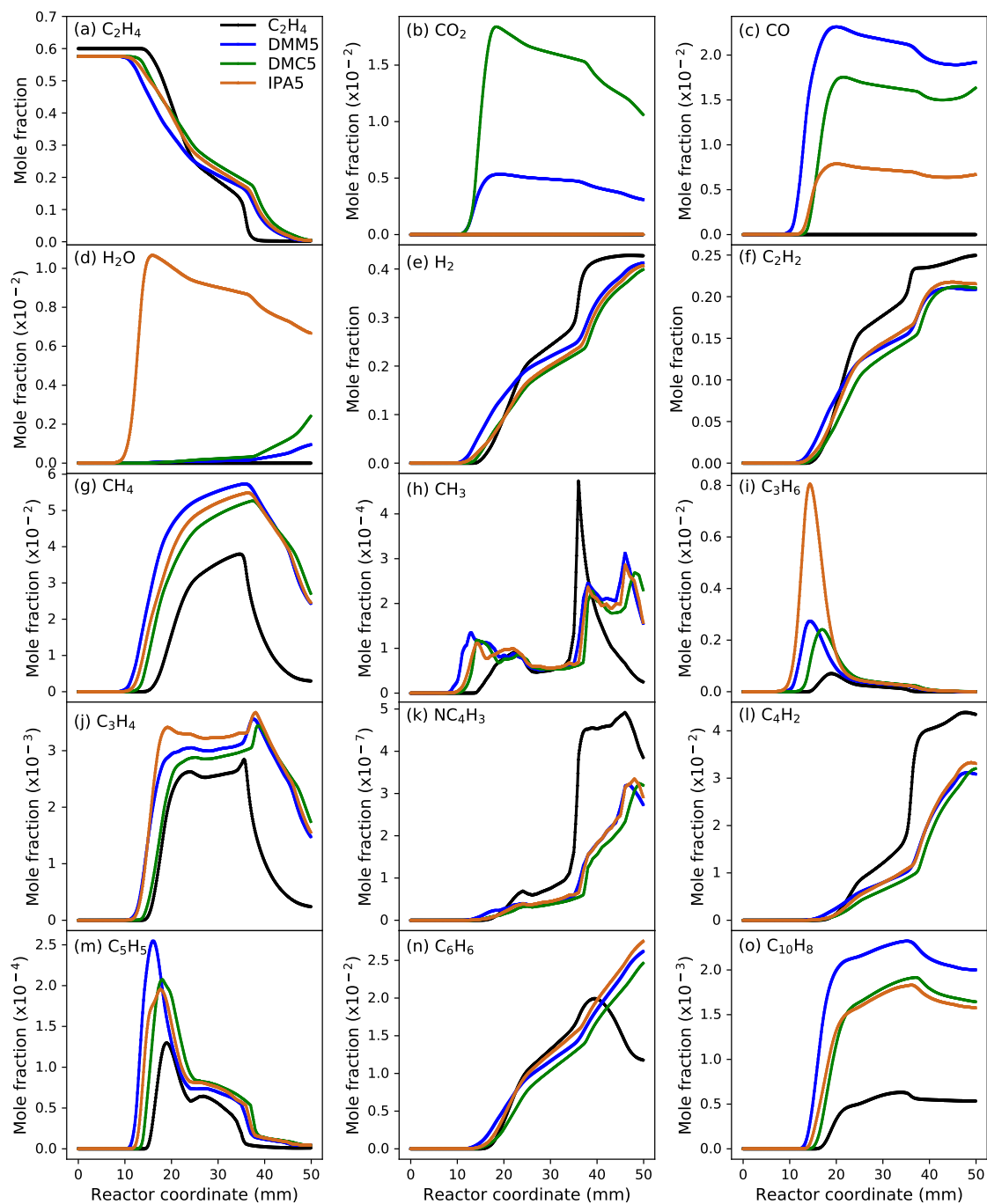


Figure SM1.4: Simulated species mole fractions during pyrolysis of the fuel blends from the C_2H_4 , DMM5, DMC5 and IPA5 flames.

The simulations were performed using the *kinetics & SRM Engine Suite* software (version 2020.1.1) [139]. The pyrolysis was modelled as occurring in a closed, atmospheric pressure Lagrangian control volume in an ideal plug flow reactor with an internal diameter of 4 mm and length of 50 mm, chosen to match the internal diameter of the burner fuel tube and average length of the flames in the current study. In each case, the measured flame temperature was imposed as a function of the reactor (length) coordinate.

SM1.2.3 Heating value and equilibrium temperature of fuel blends

Table SM1.3 shows calculated values of the lower heating value [141] and equilibrium temperature of stoichiometric mixtures of the fuel blends from the C₂H₄, DMM5, DMC5 and IPA5 flames. The calculations were performed using the *kinetics & SRM Engine Suite* software (version 2020.1.1) [139].

Table SM1.3: *Calculated lower heating value and equilibrium temperature of stoichiometric mixtures of the fuel blends.*

Fuel blend	C ₂ H ₄	DMC5	DMM5	IPA5
Lower heating value (MJ/kg)	28.3	27.9	27.5	26.9
Equilibrium temperature (K)	2326	2324	2327	2325

References

- [1] U.S. Energy Information Administration. International Energy Outlook, 2019. URL <https://www.eia.gov/outlooks/aeo/pdf/AEO2020%20Full%20Report.pdf>. Last accessed 3 June 2019.
- [2] S. J. Davis, N. S. Lewis, M. Shaner, S. Aggarwal, D. Arent, I. Azevedo, S. M. Benson, T. Bradley, J. Brouwer, Y.-M. Chiang, C. T. M. Clack, A. Cohen, S. Doig, J. Edmonds, P. Fennell, C. B. Field, B. Hannegan, B.-M. Hodge, M. I. Hoffert, E. Ingersoll, P. Jaramillo, K. S. Lackner, K. J. Mach, M. Mastrandrea, J. Ogden, P. F. Peterson, D. L. Sanchez, D. Sperling, J. Stagner, J. E. Trancik, C.-J. Yang, and K. Caldeira. Net-zero emissions energy systems. *Science*, 360(6396), 2018. doi:10.1126/science.aas9793.
- [3] K. Kohse-Höinghaus. Clean combustion: Chemistry and diagnostics for a systems approach in transportation and energy conversion. *Progress in Energy and Combustion Science*, 65:1–5, 2018. doi:10.1016/j.pecs.2017.10.001.
- [4] M. M. Wright and T. Brown. *Costs of Thermochemical Conversion of Biomass to Power and Liquid Fuels*, chapter 10, pages 337–353. John Wiley & Sons, Ltd, 2019. doi:10.1002/9781119417637.ch10.
- [5] A. Favero, A. Daigneault, and B. Sohngen. Forests: Carbon sequestration, biomass energy, or both? *Science Advances*, 6(13), 2020. doi:10.1126/sciadv.aay6792.
- [6] C. Fernández-Dacosta, L. Shen, W. Schakel, A. Ramirez, and G. J. Kramer. Potential and challenges of low-carbon energy options: Comparative assessment of alternative fuels for the transport sector. *Applied Energy*, 236:590–606, 2019. doi:10.1016/j.apenergy.2018.11.055.
- [7] U.S. Energy Information Administration. Renewables 2019, 2019. URL <https://www.iea.org/reports/renewables-2019>. Last accessed 21 June 2019.
- [8] A. Rafiee, K. R. Khalilpour, D. Milani, and M. Panahi. Trends in CO₂ conversion and utilization: A review from process systems perspective. *Journal of Environmental Chemical Engineering*, 6(5):5771 – 5794, 2018. doi:10.1016/j.jece.2018.08.065.
- [9] A. O. G. Abdalla and D. Liu. Dimethyl carbonate as a promising oxygenated fuel for combustion: A review. *Energies*, 11(6), 2018. doi:10.3390/en11061552.
- [10] H. Liu, Z. Wang, Y. Li, Y. Zheng, T. He, and J. Wang. Recent progress in the application in compression ignition engines and the synthesis technologies of polyoxymethylene dimethyl ethers. *Applied Energy*, 233-234:599 – 611, 2019. doi:10.1016/j.apenergy.2018.10.064.
- [11] S. Lonkar, Z. Fu, M. Wales, and M. Holtzapple. Creating economic incentives for waste disposal in developing countries using the MixAlco process. *Applied Biochemistry and Biotechnology*, 181(1):294–308, 2017. doi:10.1007/s12010-016-2213-6.

- [12] K. Hackbarth, P. Haltenort, U. Arnold, and J. Sauer. Recent progress in the production, application and evaluation of oxymethylene ethers. *Chemie Ingenieur Technik*, 90(10):1520–1528, 2018. doi:10.1002/cite.201800068.
- [13] M. Pan, W. Qian, Z. Zheng, R. Huang, X. Zhou, H. Huang, and M. Li. The potential of dimethyl carbonate (DMC) as an alternative fuel for compression ignition engines with different EGR rates. *Fuel*, 257:115920, 2019. doi:10.1016/j.fuel.2019.115920.
- [14] Y. Wang, A. Makwana, S. Iyer, M. Linevsky, R. J. Santoro, T. A. Litzinger, and J. O’Connor. Effect of fuel composition on soot and aromatic species distributions in laminar, co-flow flames. Part 1. Non-premixed fuel. *Combustion and Flame*, 189:443–455, 2018. doi:10.1016/j.combustflame.2017.08.011.
- [15] B. Deepanraj, G. Sankaranarayanan, N. Senthilkumar, and M. Pugazhivadivu. Influence of dimethoxymethane addition on performance, emission and combustion characteristics of the diesel engine. *International Journal of Ambient Energy*, 38(6):622–626, 2017. doi:10.1080/01430750.2016.1181568.
- [16] K. Nanthagopal, R. S. Kishna, A. E. Atabani, A. H. Al-Muhtaseb, G. Kumar, and B. Ashok. A compressive review on the effects of alcohols and nanoparticles as an oxygenated enhancer in compression ignition engine. *Energy Conversion and Management*, 203:112244, 2020. doi:10.1016/j.enconman.2019.112244.
- [17] U. I. Nda-Umar, I. Ramli, Y. H. Taufiq-Yap, and E. N. Muhamad. An overview of recent research in the conversion of glycerol into biofuels, fuel additives and other bio-based chemicals. *Catalysts*, 9(1), 2019. doi:10.3390/catal9010015.
- [18] Official Journal of the European Union. Directive (EU) 2018/2001 of the European Parliament and of the Council of 11 December 2018 on the promotion of the use of energy from renewable sources, 2018. URL <http://data.europa.eu/eli/dir/2018/2001/oj>. Last accessed 21 June 2019.
- [19] F. Hillairet, A. Djelouadji, G. Prieto, and O. Madiot. Are biofuels producers ready for the next EU energy transition?, 2019. URL <http://www.greenea.com/wp-content/uploads/2019/10/Are-biofuel-producers-ready-for-the-next-energy-transition-in-Europe-v3.pdf>. Last accessed 13 May 2020.
- [20] U.S. Department of Energy. Flexible fuel vehicles, 2020. URL https://afdc.energy.gov/vehicles/flexible_fuel.html. Last accessed 21 June 2019.
- [21] P. Aakko-Saksa, P. Koponen, P. Roslund, J. Laurikko, N.-O. Nylund, P. Karjalainen, T. Rönkkö, and H. Timonen. Comprehensive emission characterisation of exhaust from alternative fuelled cars. *Atmospheric Environment*, 236:117643, 2020. doi:10.1016/j.atmosenv.2020.117643.
- [22] H.-S. Kwon, M. H. Ryu, and C. Carlsten. Ultrafine particles: unique physicochemical properties relevant to health and disease. *Experimental & Molecular Medicine*, 52:318–328, 2020. doi:10.1038/s12276-020-0405-1.

- [23] H. R. Jonsdottir, M. Delaval, Z. Leni, A. Keller, B. T. Brem, F. Siegerist, D. Schö-
nenberger, L. Durdina, M. Elser, H. Burtscher, A. Liati, and M. Geiser. Non-
volatile particle emissions from aircraft turbine engines at ground-idle induce
oxidative stress in bronchial cells. *Communications Biology*, 2:318–328, 2019.
[doi:10.1038/s42003-019-0332-7](https://doi.org/10.1038/s42003-019-0332-7).
- [24] Z. Xia, X. Duan, S. Tao, W. Qiu, D. Liu, Y. Wang, S. Wei, B. Wang, Q. Jiang, B. Lu,
Y. Song, and X. Hu. Pollution level, inhalation exposure and lung cancer risk of
ambient atmospheric polycyclic aromatic hydrocarbons (PAHs) in Taiyuan, China.
Environmental Pollution, 173:150–156, 2013. [doi:10.1016/j.envpol.2012.10.009](https://doi.org/10.1016/j.envpol.2012.10.009).
- [25] A. C. Eriksson, C. Wittbom, P. Roldin, M. Sporre, E. Öström, P. Nilsson, J. Mar-
tinsson, J. Rissler, E. Z. Nordin, B. Svenningsson, J. Pagels, and E. Swietlicki.
Diesel soot aging in urban plumes within hours under cold dark and humid condi-
tions. *Scientific Reports*, 7:12364, 2017. [doi:10.1038/s41598-017-12433-0](https://doi.org/10.1038/s41598-017-12433-0).
- [26] J. Jones, E. Mitchell, A. Williams, E. Kumi-Barimah, G. Jose, K. Bar-
tle, N. Hondow, and A. Lea-Langton. Examination of combustion-generated
smoke particles from biomass at source: Relation to atmospheric light
absorption. *Combustion Science and Technology*, 192(1):130–143, 2020.
[doi:10.1080/00102202.2018.1557642](https://doi.org/10.1080/00102202.2018.1557642).
- [27] E. Iojoiu, V. Lauga, J. Abboud, G. Legros, J. Bonnet, P. Da Costa, J. Schob-
ing, A. Brillard, G. Leyssens, V. Tschamber, P. Anguita, J. G. Vargas, L. Retail-
leau, S. Gil, A. Giroir-Fendler, M.-L. Tarot, F. Can, D. Duprez, and X. Cour-
tois. Biofuel impact on diesel engine after-treatment: Deactivation mechanisms
and soot reactivity. *Emission Control Science and Technology*, 4:15–32, 2018.
[doi:10.1007/s40825-017-0079-x](https://doi.org/10.1007/s40825-017-0079-x).
- [28] M. Lapuerta, O. Armas, and R. García-Contreras. Effect of ethanol on blending
stability and diesel engine emissions. *Energy & Fuels*, 23(9):4343–4354, 2009.
[doi:10.1021/ef900448m](https://doi.org/10.1021/ef900448m).
- [29] C. Mata, A. Gómez, and O. Armas. The influence of ethanol-diesel blend on pol-
lutant emissions from different bus fleets under acceleration transitions. *Fuel*, 209:
322–328, 2017. [doi:10.1016/j.fuel.2017.08.018](https://doi.org/10.1016/j.fuel.2017.08.018).
- [30] G. Koçar and N. Civaş. An overview of biofuels from energy crops: Current status
and future prospects. *Renewable and Sustainable Energy Reviews*, 28:900–916,
2013. [doi:10.1016/j.rser.2013.08.022](https://doi.org/10.1016/j.rser.2013.08.022).
- [31] A. O. G. Abdalla, D. Liu, L. Zhang, X. Zhao, Y. Ying, B. Jiang, and X. He.
Soot formation and evolution in RP-3 kerosene inverse diffusion flames: Ef-
fects of flow rates and dimethyl carbonate additions. *Fuel*, 273:117732, 2020.
[doi:10.1016/j.fuel.2020.117732](https://doi.org/10.1016/j.fuel.2020.117732).
- [32] D. Mei, S. Yue, X. Zhao, K. Hielscher, and R. Baar. Effects of center of
heat release on combustion and emissions in a PCCI diesel engine fuelled
by DMC-diesel blend. *Applied Thermal Engineering*, 114:969–976, 2017.
[doi:10.1016/j.applthermaleng.2016.12.064](https://doi.org/10.1016/j.applthermaleng.2016.12.064).

- [33] J. Yang, Y. Jiang, G. Karavalakis, K. C. Johnson, S. K., D. R. Cocker, and T. D. Durbin. Impacts of dimethyl carbonate blends on gaseous and particulate emissions from a heavy-duty diesel engine. *Fuel*, 184:681–688, 2016. doi:10.1016/j.fuel.2016.07.053.
- [34] A. Arteconi, A. Mazzarini, and G. Di Nicola. Emissions from ethers and organic carbonate fuel additives: A review. *Water, Air, & Soil Pollution*, 221(1):405, 2011. doi:10.1007/s11270-011-0804-y.
- [35] Y. Li, L. Wei, Z. Tian, B. Yang, J. Wang, T. Zhang, and F. Qi. A comprehensive experimental study of low-pressure premixed C3-oxygenated hydrocarbon flames with tunable synchrotron photoionization. *Combustion and Flame*, 152(3):336–359, 2008. doi:10.1016/j.combustflame.2007.10.012.
- [36] T. S. Norton and F. L. Dryer. The flow reactor oxidation of C1–C4 alcohols and MTBE. *Symposium (International) on Combustion*, 23(1):179–185, 1991. doi:10.1016/S0082-0784(06)80257-2.
- [37] P. S. Veloo and F. N. Egolfopoulos. Studies of n-propanol, iso-propanol, and propane flames. *Combustion and Flame*, 158(3):501–510, 2011. doi:10.1016/j.combustflame.2010.10.001.
- [38] T. Ni, S.B. Gupta, and R.J. Santoro. Suppression of soot formation in ethene laminar diffusion flames by chemical additives. *Symposium (International) on Combustion*, 25(1):585–592, 1994. doi:10.1016/S0082-0784(06)80689-2.
- [39] Z.H. Huang, Y. Ren, D.M. Jiang, L.X. Liu, K. Zeng, B. Liu, and X.B. Wang. Combustion and emission characteristics of a compression ignition engine fuelled with diesel–dimethoxy methane blends. *Energy Conversion and Management*, 47(11):1402–1415, 2006. doi:10.1016/j.enconman.2005.08.020.
- [40] M. M. Maricq, R. E. Chase, D. H. Podsiadlik, W. O. Siegl, and E. W. Kaiser. The effect of dimethoxy methane additive on diesel vehicle particulate emissions. *SAE International*, 107(4):1504–1511, 1998. doi:10.4271/982572.
- [41] R. Zhu, X. Wang, H. Miao, Z. Huang, J. Gao, and D. Jiang. Performance and emission characteristics of diesel engines fueled with diesel dimethoxymethane (DMM) blends. *Energy & Fuels*, 23(1):286–293, 2009. doi:10.1021/ef8005228.
- [42] Y. Wang and S. H. Chung. Soot formation in laminar counterflow flames. *Progress in Energy and Combustion Science*, 74:152–238, 2019. doi:10.1016/j.pecs.2019.05.003.
- [43] Y. Hua, F. Liu, H. Wu, C.-F. Lee, and Y. Li. Effects of alcohol addition to traditional fuels on soot formation: A review. *International Journal of Engine Research*, 0(0):1468087420910886, 2020. doi:10.1177/1468087420910886.
- [44] L. Xu, F. Yan, W. Dai, M. Zhou, S. H. Chung, and Y. Wang. Synergistic effects on soot formation in counterflow diffusion flames of acetylene-based binary mixture fuels. *Combustion and Flame*, 216:24–28, 2020. doi:10.1016/j.combustflame.2020.02.013.

- [45] J. Abboud, J. Schobing, G. Legros, A. Matynia, J. Bonnetty, V. Tschamber, A. Brillard, G. Leyssens, and P. Da Costa. Impacts of ester's carbon chain length and concentration on sooting propensities and soot oxidative reactivity: Application to diesel and biodiesel surrogates. *Fuel*, 222:586–598, 2018. doi:10.1016/j.fuel.2018.02.103.
- [46] M. Mehl, W. J. Pitz, C. K. Westbrook, and H. J. Curran. Kinetic modeling of gasoline surrogate components and mixtures under engine conditions. *Proceedings of the Combustion Institute*, 33(1):193–200, 2011. doi:10.1016/j.proci.2010.05.027.
- [47] W. J. Pitz and C. J. Mueller. Recent progress in the development of diesel surrogate fuels. *Progress in Energy and Combustion Science*, 37(3):330–350, 2011. doi:10.1016/j.pecs.2010.06.004.
- [48] P. G. Szymkowicz and J. Benajes. Development of a diesel surrogate fuel library. *Fuel*, 222:21–34, 2018. doi:10.1016/j.fuel.2018.01.112.
- [49] C. Pichler and E. J. K. Nilsson. Analysis of important chemical pathways of n-heptane combustion in small skeletal mechanisms. *Energy & Fuels*, 34(1):758–768, 2020. doi:10.1021/acs.energyfuels.9b03263.
- [50] J. Shao, Y. Zhu, S. Wang, D. F. Davidson, and R. K. Hanson. A shock tube study of jet fuel pyrolysis and ignition at elevated pressures and temperatures. *Fuel*, 226:338–344, 2018. doi:10.1016/j.fuel.2018.04.028.
- [51] H. Wang, R. Xu, K. Wang, C. T. Bowman, R. K. Hanson, D. F. Davidson, K. Brezinsky, and F. N. Egolfopoulos. A physics-based approach to modeling real-fuel combustion chemistry - I. Evidence from experiments, and thermodynamic, chemical kinetic and statistical considerations. *Combustion and Flame*, 193:502–519, 2018. doi:10.1016/j.combustflame.2018.03.019.
- [52] X. Dong, Y. Chang, B. Niu, and M. Jia. Development of a practical reaction model of polycyclic aromatic hydrocarbon (PAH) formation and oxidation for diesel surrogate fuel. *Fuel*, 267:117159, 2020. doi:10.1016/j.fuel.2020.117159.
- [53] X. You, F. N. Egolfopoulos, and H. Wang. Detailed and simplified kinetic models of n-dodecane oxidation: The role of fuel cracking in aliphatic hydrocarbon combustion. *Proceedings of the Combustion Institute*, 32(1):403–410, 2009. doi:10.1016/j.proci.2008.06.041.
- [54] S. S. Yoon, D. H. Anh, and S. H. Chung. Synergistic effect of mixing dimethyl ether with methane, ethane, propane, and ethylene fuels on polycyclic aromatic hydrocarbon and soot formation. *Combustion and Flame*, 154(3):368–377, 2008. doi:10.1016/j.combustflame.2008.04.019.
- [55] C. S. McEnally and L. D. Pfefferle. The effects of dimethyl ether and ethanol on benzene and soot formation in ethylene nonpremixed flames. *Proceedings of the Combustion Institute*, 31(1):603–610, 2007. doi:10.1016/J.PROCI.2006.07.005.

- [56] P. Zhang, Y. Kang, Z. Wu, X. Lu, Q. Wang, and L. Mei. Effect of dimethyl ether addition on soot formation dynamics of ethylene opposed-flow diffusion flames. *Industrial & Engineering Chemistry Research*, 58(19):8370–8386, 2019. doi:10.1021/acs.iecr.9b00084.
- [57] M. Sirignano, M. Salamanca, and A. D’Anna. The role of dimethyl ether as substituent to ethylene on particulate formation in premixed and counter-flow diffusion flames. *Fuel*, 126:256–262, 2014. doi:10.1016/j.fuel.2014.02.039.
- [58] S. Trottier, H. Guo, G.J. Smallwood, and M. R. Johnson. Measurement and modeling of the sooting propensity of binary fuel mixtures. *Proceedings of the Combustion Institute*, 31(1):611–619, 2007. doi:10.1016/j.proci.2006.07.229.
- [59] Y. R. Tan, M. Salamanca, L. Pascazio, J. Akroyd, and M. Kraft. The effect of poly(oxymethylene) dimethyl ethers (PODE₃) on soot formation in ethylene/PODE₃ laminar coflow diffusion flames. *Fuel*, 283:118769, 2021. doi:10.1016/j.fuel.2020.118769.
- [60] P. Pepiot-Desjardins, H. Pitsch, R. Malhotra, S.R. Kirby, and A.L. Boehman. Structural group analysis for soot reduction tendency of oxygenated fuels. *Combustion and Flame*, 154(1):191–205, 2008. doi:10.1016/j.combustflame.2008.03.017.
- [61] J. Gau, D. Das, C. McEnally, D. Giassi, N. Kempema, and M. Long. Yale coflow diffusion flames steady flame burner, 2014. URL guilford.eng.yale.edu/yalecoflowflames/steady_burner.html. Last accessed 13 May 2019.
- [62] 4th International Sooting Flame Workshop. Laminar premixed flames, 2018. URL www.adelaide.edu.au/cet/isfworkshop/data-sets/laminar-flames#isf-4-co-flow-3-smooke-long-burner-data. PDF: www.adelaide.edu.au/cet/isfworkshop/system/files/media/documents/2019-06/2018-isf-workshop-proceedings-v4-appendices.pdf. Last accessed 29 November 2019.
- [63] P. B. Kuhn, B. Ma, B. C. Connelly, M. D. Smooke, and M. B. Long. Soot and thin-filament pyrometry using a color digital camera. *Proceedings of the Combustion Institute*, 33(1):743–750, 2011. doi:10.1016/j.proci.2010.05.006.
- [64] J. A. H. Dreyer, R. I. Slavchov, E. J. Rees, J. Akroyd, M. Salamanca, S. Mosbach, and M. Kraft. Improved methodology for performing the inverse Abel transform of flame images for color ratio pyrometry. *Applied Optics*, 58(10):2662–2670, Apr 2019. doi:10.1364/AO.58.002662.
- [65] V. A. Cundy, J. S. Morse, and D. W. Senser. Constant-tension thermocouple rake suitable for use in flame mode combustion studies. *Review of Scientific Instruments*, 57(6):1209–1210, 1986. doi:10.1063/1.1138631.
- [66] J. A. H. Dreyer, M. Poli, N. A. Eaves, M. L. Botero, J. Akroyd, S. Mosbach, and M. Kraft. Evolution of the soot particle size distribution along the centreline of an n-heptane/toluene co-flow diffusion flame. *Combustion and Flame*, 209:256–266, 2019. doi:https://doi.org/10.1016/j.combustflame.2019.08.002.

- [67] C. R. Shaddix. Correcting thermocouple measurements for radiation loss: A critical review. In *Proceedings of 33rd National Heat Transfer Conference (HTD99-282)*, 1999.
- [68] C. Irimiea, A. Faccinetto, Y. Carpentier, I.-K. Ortega, N. Nuns, E. Therssen, P. Desgroux, and C. Focsa. A comprehensive protocol for chemical analysis of flame combustion emissions by secondary ion mass spectrometry. *Rapid Communications in Mass Spectrometry*, 32(13):1015–1025, 2018. doi:10.1002/rcm.8133.
- [69] C. S. McEnally and L. D. Pfefferle. Aromatic and linear hydrocarbon concentration measurements in a non-premixed flame. *Combustion Science and Technology*, 116-117(1-6):183–209, 1996. doi:10.1080/00102209608935549.
- [70] B. Zhao, Z. Yang, J. Wang, M. V. Johnston, and H. Wang. Analysis of soot nanoparticles in a laminar premixed ethylene flame by scanning mobility particle sizer. *Aerosol Science and Technology*, 37(8):611–620, 2003. doi:10.1080/02786820300908.
- [71] J. Camacho, C. Liu, C. Gu, H. Lin, Z. Huang, Q. Tang, X. You, C. Saggese, Y. Li, H. Jung, L. Deng, I. Wlokas, and H. Wang. Mobility size and mass of nascent soot particles in a benchmark premixed ethylene flame. *Combustion and Flame*, 162(10):3810–3822, 2015. doi:10.1016/j.combustflame.2015.07.018.
- [72] H. Hepp and K. Siegmann. Mapping of soot particles in a weakly sooting diffusion flame by aerosol techniques. *Combustion and Flame*, 115(1):275–283, 1998. doi:10.1016/S0010-2180(97)00346-5.
- [73] H. Wang, X. You, A. V. Joshi, S. G. Davis, A. Laskin, F. Egolfopoulos, and C. K. Law. High-temperature combustion reaction model of $H_2/CO/C_1-C_4$ compounds. *USC Mech Version II*, 2007. URL http://ignis.usc.edu/USC_Mech_II.htm.
- [74] F. H. Vermeire, H.-H. Carstensen, O. Herbinet, F. Battin-Leclerc, G. B. Marin, and K. M. Van Geem. Experimental and modeling study of the pyrolysis and combustion of dimethoxymethane. *Combustion and Flame*, 190:270–283, 2018. doi:10.1016/j.combustflame.2017.12.001.
- [75] W. Sun, B. Yang, N. Hansen, C. K. Westbrook, F. Zhang, G. Wang, K. Moshhammer, and C. K. Law. An experimental and kinetic modeling study on dimethyl carbonate (DMC) pyrolysis and combustion. *Combustion and Flame*, 164:224–238, 2016. doi:10.1016/j.combustflame.2015.11.019.
- [76] C. Saggese, C. M. Thomas, S. W. Wagnon, G. Kukkadapu, S. Cheng, D. Kang, S. S. Goldsborough, and W.J. Pitz. An improved detailed chemical kinetic model for C3-C4 linear and iso-alcohols and their blends with gasoline at engine-relevant conditions. *Proceedings of the Combustion Institute*, 2020, in press. doi:10.1016/j.proci.2020.07.023.

- [77] C. J. Brown and G. O. Thomas. Experimental studies of shock-induced ignition and transition to detonation in ethylene and propane mixtures. *Combustion and Flame*, 117(4):861–870, 1999. doi:10.1016/S0010-2180(98)00133-3.
- [78] G. Jomaas, X. L. Zheng, D. L. Zhu, and C. K. Law. Experimental determination of counterflow ignition temperatures and laminar flame speeds of C2–C3 hydrocarbons at atmospheric and elevated pressures. *Proceedings of the Combustion Institute*, 30(1):193–200, 2005. doi:10.1016/j.proci.2004.08.228.
- [79] M. I. Hassan, K. T. Aung, O. C. Kwon, and G. M. Faeth. Properties of laminar premixed hydrocarbon/air flames at various pressures. *Journal of Propulsion and Power*, 14(4):479–488, 1998. doi:10.2514/2.5304.
- [80] F. N. Egolfopoulos, D. L. Zhu, and C. K. Law. Experimental and numerical determination of laminar flame speeds: Mixtures of C2-hydrocarbons with oxygen and nitrogen. *Symposium (International) on Combustion*, 23(1):471–478, 1991. doi:10.1016/S0082-0784(06)80293-6.
- [81] C.S. McEnally, A.M. Schaffer, M.B. Long, L.D. Pfefferle, M.D. Smooke, M.B. Colket, and R.J. Hall. Computational and experimental study of soot formation in a coflow, laminar ethylene diffusion flame. *Symposium (International) on Combustion*, 27(1):1497–1505, 1998. doi:10.1016/S0082-0784(98)80557-2.
- [82] D. Bartos, M. Sirignano, M. J. Dunn, A. D’Anna, and A. R. Masri. Soot inception in laminar coflow diffusion flames. *Combustion and Flame*, 205:180–192, 2019. doi:10.1016/j.combustflame.2019.03.026.
- [83] M.D. Smooke, M.B. Long, B.C. Connelly, M.B. Colket, and R.J. Hall. Soot formation in laminar diffusion flames. *Combustion and Flame*, 143(4):613–628, 2005. doi:10.1016/j.combustflame.2005.08.028.
- [84] B. Franzelli, M. Roussillo, P. Scoufflaire, J. Bonnet, R. Jalain, T. Dormieux, S. Candel, and G. Legros. Multi-diagnostic soot measurements in a laminar diffusion flame to assess the isf database consistency. *Proceedings of the Combustion Institute*, 37(2):1355–1363, 2019. doi:10.1016/j.proci.2018.05.062.
- [85] C. S. McEnally and L. D. Pfefferle. Flow time effects on hydrocarbon growth and soot formation in coflowing methane/air non-premixed flames. *Symposium (International) on Combustion*, 27(1):1539–1547, 1998. doi:10.1016/S0082-0784(98)80562-6.
- [86] B. A. V. Bennett, C. S. McEnally, L. D. Pfefferle, M. D. Smooke, and M. B. Colket. Computational and experimental study of axisymmetric coflow partially premixed ethylene/air flames. *Combustion and Flame*, 127(1):2004–2022, 2001. doi:10.1016/S0010-2180(01)00306-6.
- [87] M. D. Smooke, M. B. Long, B. C. Connelly, M. B. Colket, and R. J. Hall. Soot formation in laminar diffusion flames. *Combustion and Flame*, 143(4):613–628, 2005. doi:10.1016/j.combustflame.2005.08.028.

- [88] M. D. Smooke, R. J. Hall, M. B. Colket, J. Fielding, M. B. Long, C. S. McEnally, and L. D. Pfefferle. Investigation of the transition from lightly sooting towards heavily sooting co-flow ethylene diffusion flames. *Combustion Theory and Modelling*, 8(3):593–606, 2004. doi:10.1088/1364-7830/8/3/009.
- [89] J. Wu, L. Chen, P.-E. Bengtsson, J. Zhou, J. Zhang, X. Wu, and K. Cen. Effects of carbon dioxide addition to fuel on soot evolution in ethylene and propane diffusion flames. *Combustion and Flame*, 199:85–95, 2019. doi:10.1016/j.combustflame.2018.10.003.
- [90] M. Sirignano and A. D’Anna. The role of CO₂ dilution on soot formation and combustion characteristics in counter-flow diffusion flames of ethylene. *Experimental Thermal and Fluid Science*, 114:110061, 2020. doi:10.1016/j.expthermflusci.2020.110061.
- [91] K. Hayashida, T. Mogi, K. Amagai, and M. Arai. Growth characteristics of polycyclic aromatic hydrocarbons in dimethyl ether diffusion flame. *Fuel*, 90(2):493–498, 2011. doi:10.1016/j.fuel.2010.10.012.
- [92] M. Kholghy, M. Saffaripour, C. Yip, and M. J. Thomson. The evolution of soot morphology in a laminar coflow diffusion flame of a surrogate for Jet A-1. *Combustion and Flame*, 160(10):2119–2130, 2013. doi:10.1016/j.combustflame.2013.04.008.
- [93] C. S. McEnally and L. D. Pfefferle. Experimental study of nonfuel hydrocarbon concentrations in coflowing partially premixed methane/air flames. *Combustion and Flame*, 118(4):619–632, 1999. doi:10.1016/S0010-2180(99)00017-6.
- [94] C. S. McEnally and L. D. Pfefferle. The effect of nitrogen dilution on nonfuel hydrocarbons in laminar nonpremixed flames. *Combustion Science and Technology*, 151(1):133–155, 2000. doi:10.1080/00102200008924217.
- [95] A. Cuoci, A. Frassoldati, T. Faravelli, H. Jin, Y. Wang, K. Zhang, P. Glarborg, and F. Qi. Experimental and detailed kinetic modeling study of PAH formation in laminar co-flow methane diffusion flames. *Proceedings of the Combustion Institute*, 34(1):1811–1818, 2013. doi:10.1016/j.proci.2012.05.085.
- [96] K. Saito, F. A. Williams, and A. S. Gordon. Structure of laminar coflow methane–air diffusion flames. *Journal of Heat Transfer*, 108(3):640–648, 1986. doi:10.1115/1.3246984.
- [97] M. Saffaripour, A. Veshkini, M. Kholghy, and M. J. Thomson. Experimental investigation and detailed modeling of soot aggregate formation and size distribution in laminar coflow diffusion flames of jet a-1, a synthetic kerosene, and n-decane. *Combustion and Flame*, 161(3):848–863, 2014. doi:10.1016/j.combustflame.2013.10.016.
- [98] T. Kathrotia, P. Oßwald, M. Köhler, N. Slavinskaya, and U. Riedel. Experimental and mechanistic investigation of benzene formation during atmospheric pressure

- flow reactor oxidation of n-hexane, n-nonane, and n-dodecane below 1200 k. *Combustion and Flame*, 194:426–438, 2018. doi:10.1016/j.combustflame.2018.05.027.
- [99] N. Hansen, T. Kasper, B. Yang, T. A. Cool, W. Li, P. R. Westmoreland, P. Oßwald, and K. Kohse-Höinghaus. Fuel-structure dependence of benzene formation processes in premixed flames fueled by C₆H₁₂ isomers. *Proceedings of the Combustion Institute*, 33(1):585–592, 2011. doi:10.1016/j.proci.2010.05.056.
- [100] M. Frenklach. Reaction mechanism of soot formation in flames. *Physical Chemistry Chemical Physics*, 4:2028–2037, 2002. doi:10.1039/B110045A.
- [101] Y. Wang and S. H. Chung. Soot formation in laminar counterflow flames. *Progress in Energy and Combustion Science*, 74:152–238, 2019. doi:10.1016/j.pecs.2019.05.003.
- [102] H. Richter and J. B. Howard. Formation of polycyclic aromatic hydrocarbons and their growth to soot—a review of chemical reaction pathways. *Progress in Energy and Combustion Science*, 26(4):565–608, 2000. doi:10.1016/S0360-1285(00)00009-5.
- [103] C. S. McEnally, L. D. Pfefferle, B. Atakan, and K. Kohse-Höinghaus. Studies of aromatic hydrocarbon formation mechanisms in flames: Progress towards closing the fuel gap. *Progress in Energy and Combustion Science*, 32(3):247–294, 2006. doi:10.1016/j.pecs.2005.11.003.
- [104] N. Hansen, T. A. Cool, P. R. Westmoreland, and K. Kohse-Höinghaus. Recent contributions of flame-sampling molecular-beam mass spectrometry to a fundamental understanding of combustion chemistry. *Progress in Energy and Combustion Science*, 35(2):168–191, 2009. doi:10.1016/j.pecs.2008.10.001.
- [105] J. A. Miller and C. F. Melius. Kinetic and thermodynamic issues in the formation of aromatic compounds in flames of aliphatic fuels. *Combustion and Flame*, 91(1): 21–39, 1992. doi:10.1016/0010-2180(92)90124-8.
- [106] N. Hansen, S. J. Klippenstein, C. A. Taatjes, J. A. Miller, J. Wang, T. A. Cool, B. Yang, R. Yang, L. Wei, C. Huang, J. Wang, F. Qi, M. E. Law, and P. R. Westmoreland. Identification and chemistry of C₄H₃ and C₄H₅ isomers in fuel-rich flames. *The Journal of Physical Chemistry A*, 110(10):3670–3678, 2006. doi:10.1021/jp056769l.
- [107] N. Hansen, M. Schenk, K. Moshhammer, and K. Kohse-Höinghaus. Investigating repetitive reaction pathways for the formation of polycyclic aromatic hydrocarbons in combustion processes. *Combustion and Flame*, 180:250–261, 2017. doi:10.1016/j.combustflame.2016.09.013.
- [108] N. Hansen, S. J. Klippenstein, J. A. Miller, J. Wang, T. A. Cool, M. E. Law, P. R. Westmoreland, T. Kasper, and K. Kohse-Höinghaus. Identification of C₅H_x isomers in fuel-rich flames by photoionization mass spectrometry and electronic structure calculations. *The Journal of Physical Chemistry A*, 110(13):4376–4388, 2006. doi:10.1021/jp0569685.

- [109] C. F. Melius, M. E. Colvin, N. M. Marinov, W. J. Pitt, and S. M. Senkan. Reaction mechanisms in aromatic hydrocarbon formation involving the C₅H₅ cyclopentadienyl moiety. *Symposium (International) on Combustion*, 26(1):685–692, 1996. doi:10.1016/S0082-0784(96)80276-1.
- [110] L. V. Moskaleva, A. M. Mebel, and M. C. Lin. The CH₃+C₅H₅ reaction: A potential source of benzene at high temperatures. *Symposium (International) on Combustion*, 26(1):521–526, 1996. doi:10.1016/S0082-0784(96)80255-4.
- [111] J. A. Miller, M. J. Pilling, and J. Troe. Unravelling combustion mechanisms through a quantitative understanding of elementary reactions. *Proceedings of the Combustion Institute*, 30(1):43–88, 2005. doi:10.1016/j.proci.2004.08.281.
- [112] C. J. Pope and J. A. Miller. Exploring old and new benzene formation pathways in low-pressure premixed flames of aliphatic fuels. *Proceedings of the Combustion Institute*, 28(2):1519–1527, 2000. doi:10.1016/S0082-0784(00)80549-4.
- [113] A. Bhargava and P. R. Westmoreland. Measured flame structure and kinetics in a fuel-rich ethylene flame. *Combustion and Flame*, 113(3):333–347, 1998. doi:10.1016/S0010-2180(97)00208-3.
- [114] W. Li, Y. Zhang, B. Mei, Y. Li, C. Cao, J. Zou, J. Yang, and Z. Cheng. Experimental and kinetic modeling study of n-propanol and i-propanol combustion: Flow reactor pyrolysis and laminar flame propagation. *Combustion and Flame*, 207:171–185, 2019. doi:10.1016/j.combustflame.2019.05.040.
- [115] M. Baroncelli, Q. Mao, S. Galle, N. Hansen, and H. Pitsch. Role of ring-enlargement reactions in the formation of aromatic hydrocarbons. *Physical Chemistry Chemical Physics*, 22:4699–4714, 2020. doi:10.1039/C9CP05854K.
- [116] S. J. Blanksby and G. B. Ellison. Bond dissociation energies of organic molecules. *Accounts of Chemical Research*, 36(4):255–263, 2003. doi:10.1021/ar020230d.
- [117] K. Norinaga, O. Deutschmann, and K. J. Hüttinger. Analysis of gas phase compounds in chemical vapor deposition of carbon from light hydrocarbons. *Carbon*, 44(9):1790–1800, 2006. doi:10.1016/j.carbon.2005.12.050.
- [118] M. P. Ruiz, A. Callejas, A. Millera, M. U. Alzueta, and R. Bilbao. Soot formation from C₂H₂ and C₂H₄ pyrolysis at different temperatures. *Journal of Analytical and Applied Pyrolysis*, 79(1):244–251, 2007. doi:10.1016/j.jaap.2006.10.012.
- [119] H. Richter and J. B. Howard. Formation and consumption of single-ring aromatic hydrocarbons and their precursors in premixed acetylene, ethylene and benzene flames. *Physical Chemistry Chemical Physics*, 4:2038–2055, 2002. doi:10.1039/B110089K.
- [120] C. S. McEnally and L. D. Pfefferle. Comparison of non-fuel hydrocarbon concentrations measured in coflowing nonpremixed flames fueled with small hydrocarbons. *Combustion and Flame*, 117(1):362–372, 1999. doi:10.1016/S0010-2180(98)00102-3.

- [121] S. Jacobs, M. Döntgen, A. B. S. Alqaity, W. A. Kopp, L. C. Kröger, U. Burke, H. Pitsch, K. Leonhard, H. J. Curran, and K. A. Heufer. Detailed kinetic modeling of dimethoxymethane. Part II: Experimental and theoretical study of the kinetics and reaction mechanism. *Combustion and Flame*, 205:522–533, 2019. doi:10.1016/j.combustflame.2018.12.026.
- [122] P. A. Glaude, W. J. Pitz, and M. J. Thomson. Chemical kinetic modeling of dimethyl carbonate in an opposed-flow diffusion flame. *Proceedings of the Combustion Institute*, 30(1):1111–1118, 2005. doi:10.1016/j.proci.2004.08.096.
- [123] V. B. Oyeyemi, J. A. Keith, and E. A. Carter. Trends in bond dissociation energies of alcohols and aldehydes computed with multireference averaged coupled-pair functional theory. *The Journal of Physical Chemistry A*, 118(17):3039–3050, 2014. doi:10.1021/jp501636r.
- [124] Y. Georgievskii, J. A. Miller, and S. J. Klippenstein. Association rate constants for reactions between resonance-stabilized radicals: $C_3H_3 + C_3H_3$, $C_3H_3 + C_3H_5$, and $C_3H_5 + C_3H_5$. *Physical Chemistry Chemical Physics*, 9:4259–4268, 2007. doi:10.1039/B703261G.
- [125] S. E. Stein, J. A. Walker, M. M. Suryan, and A. Fahr. A new path to benzene in flames. *Symposium (International) on Combustion*, 23(1):85–90, 1991. doi:10.1016/S0082-0784(06)80245-6.
- [126] Q. Wang, G. Legros, C. Morin, M. Yao, W. Cai, and L. Jiang. Optical measurements of temperature fields in sooting flames: influence of soot self-absorption. *Applied Physics B*, 125(4):63, 2019. doi:10.1007/s00340-019-7179-y.
- [127] K. Alexandrino, Á. Millera, R. Bilbao, and M. U. Alzueta. Gas and soot formed in the dimethoxymethane pyrolysis. soot characterization. *Fuel Processing Technology*, 179:369–377, 2018. doi:10.1016/j.fuproc.2018.07.021.
- [128] J. F. Roesler, S. Martinot, C. S. McEnally, L. D. Pfefferle, J.-L. Delfau, and C. Vovelle. Investigating the role of methane on the growth of aromatic hydrocarbons and soot in fundamental combustion processes. *Combustion and Flame*, 134(3):249–260, 2003. doi:10.1016/S0010-2180(03)00093-2.
- [129] F. Yan, L. Xu, Y. Wang, S. Park, S. M. Sarathy, and S. H. Chung. On the opposing effects of methanol and ethanol addition on PAH and soot formation in ethylene counterflow diffusion flames. *Combustion and Flame*, 202:228–242, 2019. doi:10.1016/j.combustflame.2019.01.020.
- [130] N. M. Mahmoud, F. Yan, M. Zhou, L. Xu, and Y. Wang. Coupled effects of carbon dioxide and water vapor addition on soot formation in ethylene diffusion flames. *Energy & Fuels*, 33(6):5582–5596, 2019. doi:10.1021/acs.energyfuels.9b00192.
- [131] N. M. Mahmoud, W. Zhong, T. Abdalla, Q. Wang, and E. M. A. Edreis. Chemical effects of CO_2 and H_2O addition on aromatic species in ethanol/air diffusion flame. *Combustion Science and Technology*, 0(0):1–19, 2020. doi:10.1080/00102202.2020.1776705.

- [132] M. Frenklach, R. I. Singh, and A. M. Mebel. On the low-temperature limit of HACA. *Proceedings of the Combustion Institute*, 37(1):969–976, 2019. doi:10.1016/j.proci.2018.05.068.
- [133] M. Frenklach and A. M. Mebel. On the mechanism of soot nucleation. *Physical Chemistry Chemical Physics*, 22:5314–5331, 2020. doi:10.1039/D0CP00116C.
- [134] S. M. Sarathy, P. Oßwald, N. Hansen, and K. Kohse-Höinghaus. Alcohol combustion chemistry. *Progress in Energy and Combustion Science*, 44:40–102, 2014. doi:10.1016/j.pecs.2014.04.003.
- [135] C. S. McEnally and L. D. Pfefferle. An experimental study in non-premixed flames of hydrocarbon growth processes that involve five-membered carbon rings. *Combustion Science and Technology*, 131(1-6):323–344, 1998. doi:10.1080/00102209808935766.
- [136] B.-Y. Wang, Y.-X. Liu, J.-J. Weng, P. Glarborg, and Z.-Y. Tian. New insights in the low-temperature oxidation of acetylene. *Proceedings of the Combustion Institute*, 36(1):355–363, 2017. doi:10.1016/j.proci.2016.06.163.
- [137] O. Herbinet, A. Rodriguez, B. Husson, F. Battin-Leclerc, Z. Wang, Z. Cheng, and F. Qi. Study of the formation of the first aromatic rings in the pyrolysis of cyclopentene. *The Journal of Physical Chemistry A*, 120(5):668–682, 2016. doi:10.1021/acs.jpca.5b09203.
- [138] M. Salamanca, M. L. Botero, J. W. Martin, J. A. H. Dreyer, J. Akroyd, and M. Kraft. The impact of cyclic fuels on the formation and structure of soot. *Combustion and Flame*, 219:1–12, 2020. doi:10.1016/j.combustflame.2020.04.026.
- [139] CMCL Innovations. kinetics & SRM engine suite (version 2020.1.1), 2020. URL <https://cmclinnovations.com/solutions/products/kinetics/>.
- [140] David G. Goodwin, Raymond L. Speth, Harry K. Moffat, and Bryan W. Weber. Cantera: An object-oriented software toolkit for chemical kinetics, thermodynamics, and transport processes. <https://www.cantera.org>, 2018. Version 2.4.0.
- [141] J. B. Heywood. *Internal Combustion Engine Fundamentals*. McGraw-Hill, New York, 1988.